Title:

14-3-3 binding regulates Tau assembly and microtubule association.

Authors:

Janine Hochmair[1,*], Maxime C. M. van den Oetelaar[2,*], Lisa Diez[1], Lenne J. M. Lemmens[2], Renata Ponce[1], Leandre Ravatt[1], Maximilian W. Franck[1], Ekaterina Semenova[1], Satabdee Mohapatra[1,3,4], Christian Ottmann[2], Luc Brunsveld[2,#], Susanne Wegmann[1,3,4,#]

Affiliations:

[1] German Center for Neurodegenerative Diseases (DZNE), Charitéplatz 1, 10117 Berlin
[2] Laboratory of Chemical Biology, Department of Biomedical Engineering and Institute for Complex Molecular Systems, Eindhoven University of Technology
[3] Charité University Medicine, Charitéplatz 1, 10117 Berlin
[4] Einstein Center for Neuroscience (ECN), Charitéplatz 1, 10117 Berlin

Contributions:

* contributed equally
# corresponding authors

Keywords:

Tau, 14-3-3ζ, binding affinity, condensation, liquid-liquid phase separation, aggregation

Abstract

14-3-3 proteins are among the most abundant proteins in the brain and bind a large number of proteins in a phosphorylation dependent manner, including proteins prone to aggregate in neurodegenerative diseases. Binding of 14-3-3 is reported to facilitate the function, promote solubility, and coordinate the assembly of client proteins. For the microtubule-associated protein Tau, a neuronal client of 14-3-3, we show that phosphorylation-dependent stoichiometric binding of 14-3-3ζ dimers inhibits Tau assembling into biomolecular condensates, prevents its aggregation, and realizes efficient dissociation of Tau from microtubules. In contrast, at sub-stoichiometric 14-3-3 concentrations, multivalent electrostatic interactions promote the co-condensation of 14-3-3ζ with Tau in a phosphorylation-independent manner, offering an additional level in regulating the interactions of both proteins. These findings offer long-sought mechanistic insights into how 14-3-3 proteins regulate substrate solubility and highlight their importance for maintaining Tau protein functionality in the brain.

Introduction

Members of the 14-3-3 protein family are ubiquitously expressed in yeast, plant, and mammalian cells. They have hundreds of interaction partners and are important hub proteins within protein-protein interaction (PPI) networks [1]. The binding of 14-3-3 proteins is regulated by client protein phosphorylation, whereby specific motifs of two phospho-serine/phospho-threonine sites in the client jointly increase the binding affinity of 14-3-3 dimers [2–5].

14-3-3 proteins are crucially involved in neurodevelopment and synaptic health [6–9] and genetic or pharmacological reduction of 14-3-3 activity leads to deficits in synaptic and brain function [10–12]. Furthermore, 14-3-3 proteins were reported to interact with and modulate the aggregation of several proteins that accumulate in neurodegenerative protein aggregation diseases, including alpha-synuclein in Parkinson's disease [13], GFAP relevant in Alexander disease [14], and the microtubule-associated protein Tau in Alzheimer's disease and Frontotemporal dementia [15–17]. This chaperone-like function of 14-3-3 becomes particularly important in the brain - 14-3-3 constitutes about 1% (w/w) of the soluble proteome in the brain [18,19] -, where maintenance of protein function and prevention of protein misfolding and aggregation are essential for neuronal function and survival. How 14-3-3 interactions contribute to the homeostasis of aggregating brain proteins requires urgent addressing.

For Tau, phosphorylation is the major regulatory post-translational modification (PTM) that is necessary to induce the dissociation of Tau from microtubules (MTs). Tau can be phosphorylated by a number of kinases and the majority of Tau's >80 putative phosphorylation sites are located in and around the microtubule binding region [20,21]. Binding of 14-3-3 to Tau was reported to depend on the phosphorylation at two serine residues in Tau's microtubule binding region, S214 and S324 [16]. In neurodegenerative diseases, phosphorylated Tau (p-Tau) – detached from MTs – accumulates in protein aggregates in the cytosol. These observations support the current working model, in which phosphorylation-induced MT dissociation increases the concentration of p-Tau in the cytosol and thereby facilitates its aggregation. However, soluble p-Tau is abundant in the healthy human brain [22] and enriched during neurodevelopment [23,24], yet does not aggregate in these conditions. In fact, most - if not all - cellular Tau appears to be phosphorylated to some degree [25,26], indicating that efficient molecular mechanisms prevent p-Tau aggregation in the healthy brain. Because of the high 14-3-3 abundance in the brain, binding of 14-3-3 to p-Tau could provide a robust mechanism for promoting p-Tau solubility and, thereby, preventing its aggregation. In turn, misregulation of 14-3-3:Tau interactions could allow for Tau aggregation in neurodegenerative diseases. Indeed, the overall abundance of 14-3-3 proteins is reduced in AD brains [27] where they co-aggregate with Tau in neurofibrillary tangles [27].

Tau aggregation can occur through different pathways [28]: via direct aggregation of Tau into amyloid-like fibrils, initiated by FTD-mutations [29] and polyanionic co-factors [30–32], or through Tau phase separation into liquid-like condensates and the subsequent formation of oligomeric Tau seeds (liquid-to-solid transition) during condensate maturation [33–35]. Previous work suggested that the binding of 14-3-3 to Tau can modulate Tau aggregation in both directions, enhancing or inhibiting it, depending on phosphorylation [36,37]. The molecular mechanisms underlying this controversy remain unclear though.

Here, we show that 14-3-3 proteins can efficiently suppress pathological p-Tau aggregation by acting on p-Tau condensation as well as on direct amyloid-like aggregation pathways as well as on p-Tau microtubule binding. Stoichiometric binding of 14-3-3ζ dimers suppresses Tau aggregation by inhibiting Tau's 'direct' aggregation into amyloid-like fibrils and by inhibiting its liquid-like condensation, which is potentially en-route to the formation of pathological Tau species [33,34]. In contrast, in absence of specific phosphorylation-mediated binding, non-stoichiometric multivalent electrostatic interactions between 14-3-3ζ and Tau promote their co-phase separation into liquid-like condensates. Furthermore, we show that 14-3-3ζ binding facilitates efficient dissociation of p-Tau from microtubules, thereby preventing the enrichment

of free, non-chaperoned p-Tau in the cytosol at the earliest step. Together, these data highlight the importance of 14-3-3 proteins in Tau pathobiology, in which they regulate Tau condensation, aggregation, and microtubule binding based on Tau phosphorylation and thereby efficiently prevent spontaneous Tau neurotoxicity.

Results

Specific recognition by 14-3-3ζ depends on Tau phosphorylation at serine residues S214 and S324

In neurons, dimers of the 14-3-3ζ isoform were identified as interactions partners of Tau, regulated by phosphorylation of Tau at serine residues S214 (in the proline-rich domain, P1; Fig 1a) and S324 (in the third repeat, R3) [16,17,38]. To test how the binding of 14-3-3ζ is modulated by Tau phosphorylation at these residues, we determined the binding affinity of 14-3-3ζ dimers to synthetic Tau peptides carrying phosphate groups at individual or both serine residues (consisting of two short Tau sequences around S214 and S324 connected by an unstructured linker sequence; 38 aa; $Tau^{210-222(pS214)}$-GGGSGGGSGGG-$Tau^{318-331(pS324)}$; Extended Data Fig S1a). Fluorescent anisotropy measurements showed strong binding (K_D~1 μM) only in the presence of phosphorylation at both S214 and S324 residues (Tau-pS214/pS324 peptide (pS2)) (Fig 1a,b; Extended Data Fig S1b). This high binding affinity, combined with the abundance of 14-3-3 proteins in the brain (13 μg 14-3-3/mg total soluble protein [18]), could in principle enable binding of most neuronal Tau (~2 μM; [33,39,40]) if phosphorylated at pS214/pS324.
To determine further molecular details of this binding, we solved the crystal structure of 14-3-3ζ dimers in complex with the pS2 phospho-Tau peptide (Fig 1c-g; Extended Data Fig S2; Extended Data Table 1). This revealed that the pS2 peptide bound in the binding grove established after 14-3-3 dimerization, whereby pS214 and pS324 Tau residues bound to different 14-3-3ζ dimer subunits, as it is common for 14-3-3 client phospho-proteins [2].

To test whether the binding of full-length Tau to 14-3-3ζ was similarly dependent on pS214/pS324 phosphorylation, we produced recombinant Tau variants, in which S214 and S324 were replaced – individually or together – by alanine residues (S214A, S324A, S214A/S324A (TauS2A); Fig 2a). *In vitro* phosphorylation with protein kinase A (PKA) introduced phosphates at S214 and S324 in Tau, as confirmed by western blot using phospho-site specific Tau antibodies for pS214 and pS324 (Fig 2b), whereby PKA-TauS2A was phosphorylated at neither S214 nor S324. Thermal shift assays confirmed the high stability of complexes formed by 14-3-3ζ with PKA-Tau compared to PKA-TauS2A and un-phosphorylated Tau (Fig 2c). Notably, PKA phosphorylates Tau at multiple residues, apart from S214 and S324, in and next-to its repeat domain [34,41,42], which seemed to not improve binding to 14-3-3ζ. This shows the high phosphorylation site specificity of 14-3-3 proteins for their client protein binding. Together, these data show that Tau phosphorylation at S214 and S324, but not at other sites, is responsible for sequence-specific, tight binding of Tau to 14-3-3ζ dimers.

Stochiometric, sequence-specific binding of 14-3-3ζ inhibits Tau condensation

It was reported that 14-3-3 proteins can help in reducing client protein aggregation [8,43]. Whether and how this chaperoning function relies on specific client binding of 14-3-3 is unclear.

Because pathological Tau aggregation can evolve from aging liquid-like condensates [34], we investigated whether 14-3-3ζ binding would affect Tau condensation.

In the absence of 14-3-3ζ, PKA-Tau showed pronounced condensation (Fig 3a), confirming previous observations that phosphorylation generally enhances homotypic Tau condensation [33,35]. With increasing concentrations of 14-3-3ζ, however, PKA-Tau condensation was inhibited (=reduced condensate size), and at a 2:1 ratio of 14-3-3ζ (20 μM):PKA-Tau (10 μM) - resembling the condition in which all PKA-Tau monomers are in complex with 14-3-3ζ dimers -, no condensates were observed anymore. This suggested that stoichiometric binding of 14-3-3ζ dimers to PKA-Tau prevents Tau condensation. Notably, at lower 14-3-3ζ:PKA ratios, when sufficient PKA-Tau molecules where not complexed by 14-3-3z and still available for condensation, 14-3-3ζ co-condensed with PKA-Tau in the liquid-dense phase. The 14-3-3 ζ fraction found in the dense phase may hereby consist of 14-3-3z dimers bound to PKA-Tau and/or non-complexed 14-3-3ζ monomers.
To prove that the inhibition of Tau condensation depended on the binding of 14-3-3ζ to Tau phosphorylated at S214 and S324, we performed condensation experiments with the phosphorylated non-binding PKA-TauS2A (Fig 3b). In this case, 14-3-3ζ indeed did not inhibit Tau condensation. Since PKA-Tau and PKA-TauS2A differed in the phosphorylation of S214 and S324 but likely had similar overall phosphorylation levels and sites, we concluded that the pronounced inhibition of PKA-Tau condensation can be assigned to the sequence-specific binding of 14-3-3ζ involving pS214/pS324. To further confirm this idea, we used a 14-3-3ζ variant with an arginine to alanine exchange in the phospho-accepting binding pocket (14-3-3ζ R127A), which reduces the binding affinity to phospho-Tau. According to our hypothesis, 14-3-3ζ R127A inhibited PKA-Tau condensation significantly less than wildtype 14-3-3ζ (Fig 3c-e).

Tau condensation is driven by multivalent electrostatic interactions between Tau molecules themselves (homotypic co-condensation) [44] and between Tau molecules and polyanionic cofactors m (heterotypic co-condensation = coacervation) [34,45]. 14-3-3 proteins are overall acidic (pI of 14-3-3ζ = 4-5 [5]). Accordingly, the crystal structure of 14-3-3ζ dimers in complex with the Tau phospho-peptide shows many negatively charged areas on the 14-3-3ζ surface (Fig 1g). 14-3-3ζ co-condensation with Tau may thus be based on electrostatic interactions between the positively charged Tau repeat domain and negative patches on the 14-3-3ζ surface, similar to Tau coacervation with polyanions [34,46]. Indeed, 14-3-3ζ-induced Tau condensation was sensitive to increasing salt concentrations in the buffer, both in the presence and absence of the molecular crowder polyethylene glycol (PEG) (Extended Data Fig S3a,b), confirming the relevance of electrostatic interactions for the co-condensation of Tau and 14-3-3ζ.
Furthermore, sub-stoichiometric concentrations (1-5 μM 14-3-3ζ at 10 μM Tau) of 14-3-3ζ robustly induced the condensation of non-phosphorylated Tau (Extended Data Fig S3c,d) in the presence and absence of PEG, whereas higher 14-3-3ζ concentrations (>10 μM), that exceeded charge matching Tau:14-3-3ζ ratios [46], did not induce Tau condensation. A similar concentration- and charge-dependence of Tau condensation was previously described for polyanion-triggered condensation of Tau [34], which could be interpreted as a form of reentrant phase transition behavior [46–48] (the transition from a one-phase into a two-phase system and back into a one-phase system depending only on one parameter; for Tau: the anionic coacervation partner concentration).

In contrast, 14-3-3ζ failed to induce PKA-Tau condensation in the absence of PEG (Extended Data Fig S3f), likely because of specific PKA-Tau:14-3-3z binding or because PKA phosphorylation has added extra negative charges on Tau that disfavor electrostatic interactions necessary for Tau:14-3-3ζ coacervation. We previously observed a similar effect for the co-condensation of PKA-Tau with RNA [34]. The presence of molecular crowding agents, e.g., PEG, can overcome this problem by increasing the apparent protein concentration through excluded volume effects, thereby favoring protein-protein interactions leading to LLPS.

Together, these data suggest that 14-3-3ζ co-condenses with Tau based on multivalent electrostatic interactions between the two proteins. Stoichiometric binding pocket interactions of 14-3-3ζ dimers with Tau monomers phosphorylated at S214 and S324 make Tau molecules unavailable for multivalent interactions needed for LLPS and, therefore, counteract their co-condensation. The suppression of biomolecular condensation by 14-3-3 binding has been suggested for other physiological and disease-associated 14-3-3 binding partners [49,50], however, the molecular mechanisms behind this process previously remained uncertain.

Tau:14-3-3ζ binding interferes with molecular mobility in condensates

To elucidate whether the stoichiometric binding of p-Tau and 14-3-3ζ would affect their molecular mobility within condensates, we performed fluorescence recovery after photobleaching (FRAP) measurements on Tau:14-3-3ζ condensates, using combinations of Tau and 14-3-3ζ variants with different binding activities.

First, we tested how 14-3-3ζ concentration would influence Tau mobility inside condensates. In the absence of 14-3-3ζ, Tau and PKA-Tau showed similar FRAP, which in both cases decreased with increasing 14-3-3 concentrations (Extended Data Fig S4a,b; 10 μM Tau including 2% Tau-DyLight488; 0, 1, 5 or 10 μM 14-3-3ζ including 2% 14-3-3ζ-DyLight650).

We then compared how 14-3-3ζ binding affinity would influence Tau mobility inside condensates. In non-binding conditions (PKA-TauS2A (mobile fraction: 64%, $t_{1/2}$=7s) and unphosphorylated Tau (mobile fraction: 61%, $t_{1/2}$=4s)), the fraction of mobile Tau molecules was higher than in binding conditions (PKA-Tau with 14-3-3ζ (mobile fraction: 50%, $t_{1/2}$=6s); Fig 3f, left; Extended Data Fig S4c,d). The non-binding mutant 14-3-3ζ^{R127A} partially rescued PKA-Tau FRAP (PKA-Tau+14-3-3ζR127A (mobile fraction: 54%, $t_{1/2}$=3s) vs. PKA-Tau+14-3-3ζ (mobile fraction: 50%, $t_{1/2}$=6s)). Notably, PKA-TauS2A showed slow recovery with 14-3-3ζ, similar to PKA-Tau, suggesting that Tau phosphorylation (aside from S214 and S324) may generally increase multivalent interactions in Tau condensates, thereby reducing Tau molecular mobility.

FRAP of 14-3-3ζ in the condensates revealed a similar trend, with vivid recovery for non-binding conditions (Tau:14-3-3ζ (mobile fraction: 85%, $t_{1/2}$=7s) and PKA-TauS2A:14-3-3ζ (mobile fraction: 72%, $t_{1/2}$=13s)), which was reduced in binding conditions (PKA-Tau:14-3-3ζ (mobile fraction: 50%, $t_{1/2}$=17s); Fig 3f, right). In PKA-Tau:14-3-3ζ^{R127A} condensates with reduced binding, 14-3-3ζ fluorescence recovered fast but maintained a low percentage of mobile molecules (mobile fraction: 46%, $t_{1/2}$=4s). Collectively, these data suggest that the binding of 14-3-3 partially immobilizes Tau molecules - or reduces their molecular flexibility – inside liquid-condensed phases, which likely also changes the physical properties of Tau condensates.

230 We previously showed that aging of Tau and phospho-Tau condensates also leads to a
231 decrease in Tau molecular mobility (by FRAP), reminiscent of a liquid-to-solid transition
232 induced by supramolecular polymerization processes, and that this process produces Tau
233 species with pathological seeding competence [33,34]. To test whether the presence of 14-3-3ζ
234 would influence Tau condensate aging process, we performed FRAP on Tau and PKA-Tau
235 condensates in the absence and at sub-stoichiometric 14-3-3ζ concentration (14-3-3:Tau ratio
236 < 0.5:1), Extended Data Fig S5) at 2 h, and 6h after condensate formation. Both Tau or PKA-
237 Tau condensates showed a loss in FRAP in the absence and the presence of 14-3-3ζ,
238 suggesting that the pure presence of 14-3-3 did not prevent Tau and PKA-Tau condensate
239 aging (loss of FRAP over time).
240

241 ***Out-competing stochiometric p-Tau binding re-enables its multivalent condensation***
242 ***with 14-3-3ζ***

243 14-3-3 proteins have a number of condensing protein interaction partners in the cytosol that
244 simultaneously compete for their binding. Changes in the binding affinity of individual
245 interactions partners, regulated by their (de-)phosphorylation, may therefore influence the
246 condensation of others. To test this idea, we used the Tau peptide pS2 (Fig 1a, Extended Data
247 Fig S1a) to compete against PKA-Tau for the binding of 14-3-3ζ (Fig 4a). We hypothesized
248 that if PKA-Tau:14-3-3ζ co-condensation is inhibited due to their specific binding, competing-
249 out PKA-Tau with the pS2 peptide should re-enable PKA-Tau condensate formation.
250

251 Indeed, at equimolar concentrations of PKA-Tau and 14-3-3ζ, where no (or very little)
252 condensation occurs (Fig 2b, Fig 4b), increasing the pS2 peptide concentration to 10-40 μM
253 induced the formation of PKA-Tau:14-3-3ζ condensates (Fig 4b,c). These condensates also
254 contained the pS2 peptide (Fig 4d), indicating that PKA-Tau can co-condense with 14-3-3ζ that
255 is bound to another substrate (here pS2; Fig 4d). These results also corroborate the
256 observation that Tau:14-3-3ζ co-condensation is driven by multivalent electrostatic interactions
257 via residues outside of the 14-3-3 binding pocket. Interestingly, a further increase of the pS2
258 concentration >40 μM reduced PKA-Tau condensation, suggesting that pS2 induced a
259 reentrant phase transition of PKA-Tau, similar to what we observed for Tau at increasing 14-
260 3-3ζ concentrations (Extended Data Fig S3a). These observations support the idea that the
261 competition between 14-3-3 binding partners – here PKA-Tau *versus* pS2 – influences their
262 solubility. In addition, 14-3-3 clients can co-condense with 14-3-3 bound to another target,
263 which enables 14-3-3 proteins to generate phase separated catalytic hubs.
264

265 ***14-3-3ζ binding prevents Tau aggregation***

266 The high levels of 14-3-3 proteins in the brain may assist in efficiently preventing p-Tau
267 aggregation. In this case, a reduced availability of chaperoning 14-3-3, or the inhibition of 14-
268 3-3 binding to Tau, should enable or enhance Tau aggregation of otherwise stably complexed
269 soluble p-Tau. To test this idea, we used primary hippocampal mouse neurons, in which Tau
270 is phosphorylated at S214 and S324 (Fig 4f), a prerequisite for 14-3-3ζ binding. Expression of
271 pro-aggregant FTD-mutant human Tau (eGFP-Tau$^{P301L/S320F}$), using AAVs, led to spontaneous
272 Tau aggregation into neurofibrillary tangle-like, fibrillar aggregates, in a subset (~2%) of
273 neurons (Fig 4g,h). When treating these neurons with BV02, an inhibitor of 14-3-3 binding to
274 its phosphorylated clients [51,52], Tau$^{P301L/S320F}$ aggregation increased in a dose dependent

manner (~4% cells with aggregates at 10 μM BV02, ~7% cells with aggregates at 40 μM BV02). This suggested that the binding of 14-3-3 to p-Tau actively suppressed FTD-mutant Tau aggregation in neurons. Of note, this analysis involved the normalization of Tau aggregates to all cells in culture, including neurons and glia cells, and therefor may underestimate the increase of Tau aggregation in neurons. In *in vitro* assays of heparin-induced aggregation of another pro-aggregant mutant Tau, $Tau^{\Delta K280}$, the presence of 14-3-3ζ reduced PKA-Tau aggregation (Fig 4i), which confirmed the observations in neurons.

14-3-3ζ binding enables dissociation of phospho-Tau from microtubules

Tau has a high affinity to MTs when not phosphorylated (Tau:MTs $K_D \approx 1$ μM), which is mediated by the Tau repeat domain and its flanking regions (P2 and R'; Fig 1a; [53]). This binding affinity decreases upon phosphorylation of different serine and threonine residues in these regions, and Tau phosphorylation is widely thought to be sufficient to induce the dissociation of Tau from MTs [26]. Our data show that 14-3-3ζ has a similarly high affinity to Tau phosphorylated at S214 and S324 (pS2:14-3-3ζ $K_D \approx 1$ μM). The affinity of PKA-Tau to 14-3-3 may thus be higher than that to MTs, which led us to speculate that 14-3-3ζ could function as a scavenger of p-Tau in order to prevent the potential condensation and aggregation of free p-Tau in the cytosol (Fig 5a). In this scenario, the efficient formation of 14-3-3ζ:p-Tau complexes could sequester p-Tau from MTs, and thereby decrease the amount of p-Tau on MTs.

We tested whether the presence of 14-3-3 would decrease the amount of PKA-Tau attached to MTs. Indeed, in *in vitro* MTs pelleting assays, we found that the presence of 14-3-3ζ significantly decreased the fraction of PKA-Tau bound to MTs (=more PKA-Tau in the supernatant), whereas MT binding of non-phosphorylated Tau was unaffected (Fig 5b,c).
To confirm these results, we *in vitro* polymerized MTs in the presence of fluorescently labeled Tau or PKA-Tau and visualized Tau binding by confocal microscopy [34,54]. We observed the binding of Tau to MT bundles for non-phosphorylated Tau, PKA-Tau, and PKA-TauS2A (Fig 5d-f). This indicated that phosphorylation by PKA alone was not sufficient to completely detach Tau from MTs. This was in line with the results from the MT pelleting assay, where most PKA-Tau remained bound to MTs in the absence of 14-3-3ζ. When performing the MT imaging assay in the presence of 14-3-3ζ, however, non-phosphorylated Tau (not binding 14-3-3ζ) still co-localized with MT bundles, whereas PKA-Tau (binding 14-3-3ζ) was now absent from MTs (Fig 5g,h). This supported the idea that 14-3-3ζ binding promoted the dissociation of PKA-Tau from MTs. By using PKA-TauS2A, which does not bind 14-3-3ζ, we could rescue the Tau binding to MTs (Fig 5i), confirming that the specific binding of PKA-Tau to 14-3-3ζ is the molecular mechanism behind the sequestration of p-Tau from MTs.

In conditions where Tau did not bind 14-3-3ζ (Tau and PKA-TauS2A), we observed condensates containing Tau, 14-3-3ζ, and tubulin forming the center of "MT asters" (Fig 5g,i). Unlike Tau, 14-3-3ζ was confined to these condensates and did not coat the outgrowing MTs. We previously observed similar MT outgrowth from Tau condensates in the presence of RNA [34]. Interestingly, like 14-3-3, RNA also reduces Tau binding to MTs, leading to a destabilization of MTs [34,55]. The co-condensation of different negatively charged interaction partners with Tau – e.g., 14-3-3ζ and RNA – may be involved in modulating Tau binding to MTs and thereby MT stability.

Discussion

Tau protein aggregation is a pathological hallmark in over 20 neurodegenerative brain diseases. However, all tauopathies – even frontotemporal dementia variants caused by pro-aggregation mutations in the Tau gene, MAPT - are age-related and occur only later in life. *In vitro* studies on purified Tau proteins predict a spontaneous aggregation of Tau in hours to days, depending on the presence of PTMs, mutations, and polyanionic co-factors like heparin. It is, so far, unclear what promotes the high solubility and prevents the aggregation of Tau observed the brain, despite its rather high physiological concentration (~2 μM; [33,39,40]). Our data now reveals that phospho-site specific, stoichiometric binding of 14-3-3ζ dimers to Tau phosphorylated at S214 and S324 efficiently keeps p-Tau in solution by actively preventing its assembly into liquid-like condensates and amyloid-like fibrils.

At stoichiometric or higher ratios (14-3-3:Tau ≥ 2:1), when all p-Tau molecules are in complex with 14-3-3 dimers, condensate formation, which generally requires molecular flexibility and relies on multivalent electrostatic interactions between Tau and 14-3-3, is blocked (Fig 3g, Fig 6). High, stoichiometric 14-3-3 concentrations, as they are found in the brain, could therefore efficiently inhibit p-Tau condensation and thereby prevent the formation of pathological Tau "seeds" in Tau condensates [33–35].

Negative modulation of phase separation by 14-3-3 was recently reported for different RNA binding proteins [49]. Using the example of Tau, we can show that this effect can be tuned through the binding affinity of 14-3-3, which depends on site-specific phosphorylation of 14-3-3 client proteins.

Furthermore, we find that the presence of other clients that compete for the interaction with 14-3-3 can modulate the phase separation of Tau, and likely other 14-3-3 binders. This reveals a novel concept of how cellular biomolecular condensation of proteins can be tuned in "cis" by modulating the binding affinity of other proteins to 14-3-3, simply by adding phosphorylation at specific, individual serine residues. The formation of biomolecular condensates of 14-3-3 interactors can, thus, be tuned not only by phosphorylation of the respective client, but also by phosphorylation of other clients. This equips the cell with a mechanism of conditional condensation of 14-3-3 interaction partners based on their binding affinity and availability. Since 14-3-3 clients are able to co-condense with 14-3-3 bound to another target (herein, PKA-Tau with 14-3-3ζ:pS2 peptide complex), 14-3-3 proteins can generate phase separated catalytic hubs.

However, these observations also imply that a dysregulation of 14-3-3 client protein phosphorylation leading to the dissociation of 14-3-3 dimers from aggregating proteins, e.g., Tau, can enable pro-pathological protein condensation and aggregation. Indeed, reducing the affinity of 14-3-3 to Tau, e.g., by inhibiting phosphorylation at S214/S324, or blocking the interaction of 14-3-3 with p-Tau, e.g., pharmacologically with BV02, reduces the chaperoning effect of 14-3-3 and allows Tau to phase separate and aggregate in the cytosol. Reduced levels of 14-3-3 proteins in AD brains [56] may thus be involved in promoting neurotoxic p-Tau accumulation and aggregation.

Since phosphorylation on S214 and S324 is crucial to enable the binding and "restraining" of Tau by 14-3-3ζ, our findings have controversial implications for using unspecific or insufficiently characterized kinase inhibitors as a treatment approach to inhibit Tau aggregation in the brain. General blocking of Tau phosphorylation could result in reduced complexation of Tau with chaperoning molecules like 14-3-3 and, therefore, exert opposing effects by increasing aggregation and toxicity. Instead, increasing 14-3-3ζ binding activity to Tau may be help to prevent aberrant Tau aggregation as a therapeutic approach. Similar approaches may

also be explored for neurodegenerative conditions involving other condensing and aggregating client proteins of 14-3-3, for example, a-synuclein in Parkinson's disease [57].

At sub-stoichiometric 14-3-3 concentrations (14-3-3ζ:p-Tau ratio < 2:1), unbound Tau molecules co-condense with 14-3-3ζ:p-Tau complexes. In fact, 14-3-3ζ seems to promote the condensation of Tau based on electrostatic interactions, similar to what has been reported for Tau condensation with polyanionic RNA and heparin [34,45]. The predominantly negatively charged surface of 14-3-3ζ (Fig. 1g), and the observation that Tau phosphorylation (adding negative charges to Tau) inhibits PKA-Tau:14-3-3ζ coacervation, suggest that these interactions are engaging the positively-charged repeat domain of Tau. Interestingly, FRAP of Tau:14-3-3ζ condensates inversely correlated with the binding affinity of 14-3-3 to Tau - to some degree -, indicating a reduced molecular diffusion of Tau:14-3-3ζ complexes in and into condensates, which could be due to the larger molecular weight of Tau:14-3-3ζ complexes (compared to individual Tau and 14-3-3- monomers) and/or differences in their electrostatic interactions with remaining unbound Tau molecules inside condensates. Notably, Tau:14-3-3ζ condensates showed a decrease of FRAP over time similar to condensates without 14-3-3ζ, indicating that co-condensation of 14-3-3ζ did not abolish potentially pro-pathological liquid-to-gel transition of Tau condensates [33]. In the cellular context, the formation of Tau:14-3-3-condensates, for example, due to reduced 14-3-3 levels or binding competition with other 14-3-3 clients, may thus induce Tau aggregation.

In this regard, our data suggest that co-condensation of Tau with 14-3-3 in cells could be limited/prevented based on Tau binding competition between MTs and 14-3-3. Whereas MTs have a higher affinity to non-phosphorylated Tau compared to p-Tau, the opposite is the case for 14-3-3. When Tau becomes phosphorylated to dissociate from MTs, the higher binding affinity of 14-3-3 to p-Tau allows it to "scavenge" p-Tau from MTs. This not only ensures that p-Tau leaves the MT surface but it also limits the availability of p-Tau for unwanted interactions and assembly reactions (condensation and aggregation) in the cytosol.

In summary, our results propose a model, in which 14-3-3 proteins make an important contribution to cellular Tau solubility and function: Stoichiometric, phosphorylation-dependent binding of 14-3-3ζ enables the dissociation of Tau phosphorylated at pS214/pS324 from the MT surface, which is important to enable MT dynamics. At the same time, the binding of 14-3-3 ensures the solubility of p-Tau in the cytosol by suppressing its condensation as well as its aggregation. The seeming-less "handing-over" of Tau between the MT surface and chaperoning 14-3-3 dimers would explain why pathological Tau aggregation is observed when 14-3-3 levels and other complementary homeostatic mechanisms start to deteriorate, for example in the aging brain. These new insights into the role of 14-3-3 proteins in keeping aggregating proteins, like Tau, in control could open the way for new therapeutic approaches based on increasing the affinity of 14-3-3 to phosphorylated clients with aggregation potential. Designing a "molecular glue" that stabilizes 14-3-3:p-Tau interactions and facilitates Tau solubility, even in situations of reduced protein homeostasis, may be able to prevent or at least reduce Tau aggregation and toxicity in the brain.

References

1. Morrison, D. K. The 14-3-3 proteins: integrators of diverse signaling cues that impact cell fate and cancer development. *Trends Cell Biol* **19**, 16–23 (2009).

2. Obsilova, V. & Obsil, T. Structural insights into the functional roles of 14-3-3 proteins. *Front Mol Biosci* **9**, (2022).
3. Sluchanko, N. N. Reading the phosphorylation code: binding of the 14-3-3 protein to multivalent client phosphoproteins. *Biochem J* **477**, 1219–1225 (2020).
4. Stevers, L. M., de Vink, P. J., Ottmann, C., Huskens, J. & Brunsveld, L. A Thermodynamic Model for Multivalency in 14-3-3 Protein-Protein Interactions. *J Am Chem Soc* **140**, 14498–14510 (2018).
5. Yaffe, M. B. *et al.* The structural basis for 14-3-3:phosphopeptide binding specificity. *Cell* **91**, 961–971 (1997).
6. Shimada, T., Fournier, A. E. & Yamagata, K. Neuroprotective function of 14-3-3 proteins in neurodegeneration. *Biomed Res Int* **2013**, (2013).
7. Kaplan, A. *et al.* Small-Molecule Stabilization of 14-3-3 Protein-Protein Interactions Stimulates Axon Regeneration. *Neuron* **93**, 1082-1093.e5 (2017).
8. Cho, E. & Park, J. Y. Emerging roles of 14-3-3γ in the brain disorder. *BMB Rep* **53**, 500–511 (2020).
9. Zhang, J. & Zhou, Y. 14-3-3 Proteins in Glutamatergic Synapses. *Neural Plast* **2018**, (2018).
10. Cho, E., Park, J., Hwang, E. M., Kim, H. W. & Park, J. Y. 14-3-3γ haploinsufficiency leads to altered dopamine pathway and Parkinson's disease-like motor incoordination in mice. *Mol Brain* **16**, 1–18 (2023).
11. Graham, K., Zhang, J., Qiao, H., Wu, Y. & Zhou, Y. Region-specific inhibition of 14-3-3 proteins induces psychomotor behaviors in mice. *npj Schizophrenia 2019 5:1* **5**, 1–8 (2019).
12. Qiao, H., Foote, M., Graham, K., Wu, Y. & Zhou, Y. 14-3-3 Proteins Are Required for Hippocampal Long-Term Potentiation and Associative Learning and Memory. *The Journal of Neuroscience* **34**, 4801 (2014).
13. Giusto, E., Yacoubian, T. A., Greggio, E. & Civiero, L. Pathways to Parkinson's disease: a spotlight on 14-3-3 proteins. *NPJ Parkinsons Dis* **7**, (2021).
14. Li, H. *et al.* 14-3-3γ affects dynamics and integrity of glial filaments by binding to phosphorylated GFAP. *J Cell Sci* **119**, 4452–4461 (2006).
15. Qureshi, H. Y. *et al.* Interaction of 14-3-3ζ with microtubule-associated protein tau within Alzheimer's disease neurofibrillary tangles. *Biochemistry* **52**, 6445–6455 (2013).
16. Neves, J. F. *et al.* Phosphorylated full-length Tau interacts with 14-3-3 proteins via two short phosphorylated sequences, each occupying a binding groove of 14-3-3 dimer. *FEBS Journal* **288**, 1918–1934 (2021).
17. Chen, Y. *et al.* 14-3-3/Tau Interaction and Tau Amyloidogenesis. *J Mol Neurosci* **68**, 620–630 (2019).
18. Boston, P. F., Jackson, P. & Thompson, R. J. Human 14-3-3 protein: radioimmunoassay, tissue distribution, and cerebrospinal fluid levels in patients with neurological disorders. *J Neurochem* **38**, 1475–1482 (1982).
19. Berg, D., Holzmann, C. & Riess, O. 14-3-3 proteins in the nervous system. *Nature Reviews Neuroscience 2003 4:9* **4**, 752–762 (2003).
20. Wegmann, S., Biernat, J. & Mandelkow, E. A current view on Tau protein phosphorylation in Alzheimer's disease. *Curr Opin Neurobiol* **69**, 131–138 (2021).
21. Drepper, F. *et al.* A combinatorial native MS and LC-MS/MS approach reveals high intrinsic phosphorylation of human tau but minimal levels of other key modifications. *Journal of Biological Chemistry* **295**, 18213–18225 (2020).
22. Wesseling, H. *et al.* Tau PTM Profiles Identify Patient Heterogeneity and Stages of Alzheimer's Disease. *Cell* **183**, 1699-1713.e13 (2020).
23. Brion, J. P., Octave, J. N. & Couck, A. M. Distribution of the phosphorylated microtubule-associated protein tau in developing cortical neurons. *Neuroscience* **63**, 895–909 (1994).
24. Kenessey, A. & Yen, S. H. C. The extent of phosphorylation of fetal tau is comparable to that of PHF-tau from Alzheimer paired helical filaments. *Brain Res* **629**, 40–46 (1993).

25. Lindwall, G. & Cole, R. D. Phosphorylation affects the ability of tau protein to promote microtubule assembly. *Journal of Biological Chemistry* **259**, 5301–5305 (1984).
26. Noble, W., Hanger, D. P., Miller, C. C. J. & Lovestone, S. The importance of tau phosphorylation for neurodegenerative diseases. *Front Neurol* **4 JUL**, (2013).
27. Umahara, T. *et al.* 14-3-3 proteins and zeta isoform containing neurofibrillary tangles in patients with Alzheimer's disease. *Acta Neuropathol* **108**, 279–286 (2004).
28. Lin, Y., Fichou, Y., Zeng, Z., Hu, N. Y. & Han, S. Electrostatically Driven Complex Coacervation and Amyloid Aggregation of Tau Are Independent Processes with Overlapping Conditions. *ACS Chem Neurosci* **11**, 615–627 (2020).
29. Von Bergen, M. *et al.* Mutations of Tau Protein in Frontotemporal Dementia Promote Aggregation of Paired Helical Filaments by Enhancing Local β-Structure. *Journal of Biological Chemistry* **276**, 48165–48174 (2001).
30. Kampers, T., Friedhoff, P., Biernat, J., Mandelkow, E. M. & Mandelkow, E. RNA stimulates aggregation of microtubule-associated protein tau into Alzheimer-like paired helical filaments. *FEBS Lett* **399**, 344–349 (1996).
31. Ramachandran, G. & Udgaonkar, J. B. Understanding the kinetic roles of the inducer heparin and of rod-like protofibrils during amyloid fibril formation by tau protein. *Journal of Biological Chemistry* **286**, 38948–38959 (2011).
32. Goedert, M. *et al.* Assembly of microtubule-associated protein tau into Alzheimer-like filaments induced by sulphated glycosaminoglycans. *Nature 1996 383:6600* **383**, 550–553 (1996).
33. Wegmann, S. *et al.* Tau protein liquid–liquid phase separation can initiate tau aggregation. *EMBO J* **37**, e98049 (2018).
34. Hochmair, J. *et al.* Molecular crowding and RNA synergize to promote phase separation, microtubule interaction, and seeding of Tau condensates. *EMBO J* **41**, e108882 (2022).
35. Kanaan, N. M., Hamel, C., Grabinski, T. & Combs, B. Liquid-liquid phase separation induces pathogenic tau conformations in vitro. *Nat Commun* **11**, (2020).
36. Sluchanko, N. N. & Gusev, N. B. Probable Participation of 14-3-3 in Tau Protein Oligomerization and Aggregation. *Journal of Alzheimer's Disease* **27**, 467–476 (2011).
37. Hernández, F., Cuadros, R. & Avila, J. Zeta 14-3-3 protein favours the formation of human tau fibrillar polymers. *Neurosci Lett* **357**, 143–146 (2004).
38. Joo, Y. *et al.* Involvement of 14-3-3 in tubulin instability and impaired axon development is mediated by Tau. *FASEB J* **29**, 4133–4144 (2015).
39. Khatoon, S., Grundke-Iqbal, I. & Iqbal, K. Brain Levels of Microtubule-Associated Protein τ Are Elevated in Alzheimer's Disease: A Radioimmuno-Slot-Blot Assay for Nanograms of the Protein. *J Neurochem* **59**, 750–753 (1992).
40. Butner, K. A. & Kirschner, M. W. Tau protein binds to microtubules through a flexible array of distributed weak sites. *Journal of Cell Biology* **115**, 717–730 (1991).
41. Liu, F. *et al.* PKA modulates GSK-3β- and cdk5-catalyzed phosphorylation of tau in site- and kinase-specific manners. *FEBS Lett* **580**, 6269–6274 (2006).
42. Martin, L. *et al.* Tau protein kinases: Involvement in Alzheimer's disease. *Ageing Res Rev* **12**, 289–309 (2013).
43. Giusto, E., Yacoubian, T. A., Greggio, E. & Civiero, L. Pathways to Parkinson's disease: a spotlight on 14-3-3 proteins. *npj Parkinson's Disease 2021 7:1* **7**, 1–14 (2021).
44. Boyko, S., Qi1, X., Chen, T. H., Surewicz, K. & Surewicz, W. K. Liquid-liquid phase separation of tau protein: The crucial role of electrostatic interactions. *Journal of Biological Chemistry* **294**, 11054–11059 (2019).
45. Zhang, X. *et al.* RNA stores tau reversibly in complex coacervates. *PLoS Biol* **15**, (2017).
46. Lin, Y. *et al.* Narrow equilibrium window for complex coacervation of tau and RNA under cellular conditions. *Elife* **8**, 1–21 (2019).
47. Babinchak, W. M. *et al.* Small molecules as potent biphasic modulators of protein liquid-liquid phase separation. *Nature Communications 2020 11:1* **11**, 1–15 (2020).

48. Banerjee, P. R., Milin, A. N., Moosa, M. M., Onuchic, P. L. & Deniz, A. A. Reentrant phase transition drives dynamic substructure formation in ribonucleoprotein droplets. *Angew Chem Int Ed Engl* **56**, 11354 (2017).
49. Segal, D. *et al.* A central chaperone-like role for 14-3-3 proteins in human cells. *Mol Cell* **83**, 974-993.e15 (2023).
50. Fehilly, J. *et al.* Condensate formation of the human RNA-binding protein SMAUG1 is controlled by its intrinsically disordered regions and interactions with 14-3-3 proteins. *bioRxiv* 2023.02.09.527857 (2023) doi:10.1101/2023.02.09.527857.
51. Corradi, V. *et al.* Identification of the first non-peptidic small molecule inhibitor of the c-Abl/14-3-3 protein-protein interactions able to drive sensitive and Imatinib-resistant leukemia cells to apoptosis. *Bioorg Med Chem Lett* **20**, 6133–6137 (2010).
52. Iralde-Lorente, L. *et al.* Chemically stable inhibitors of 14-3-3 protein-protein interactions derived from BV02. *J Enzyme Inhib Med Chem* **34**, 657–664 (2019).
53. Mukrasch, M. D. *et al.* The 'jaws' of the tau-microtubule interaction. *J Biol Chem* **282**, 12230–12239 (2007).
54. Hernández-Vega, A. *et al.* Local Nucleation of Microtubule Bundles through Tubulin Concentration into a Condensed Tau Phase. *Cell Rep* **20**, 2304–2312 (2017).
55. Bryan, J., Nagle, B. W. & Doenges, K. H. Inhibition of tubulin assembly by RNA and other polyanions: evidence for a required protein. *Proc Natl Acad Sci U S A* **72**, 3570–3574 (1975).
56. Gu, Q., Cuevas, E., Raymick, J., Kanungo, J. & Sarkar, S. Downregulation of 14-3-3 Proteins in Alzheimer's Disease. *Mol Neurobiol* **57**, 32–40 (2020).
57. Underwood, R. *et al.* 14-3-3 mitigates alpha-synuclein aggregation and toxicity in the in vivo preformed fibril model. *Acta Neuropathol Commun* **9**, 1–16 (2021).
58. Barghorn, S., Biernat, J. & Mandelkow, E. Purification of recombinant tau protein and preparation of alzheimer-paired helical filaments in vitro. *Methods in Molecular Biology* **299**, 35–51 (2005).
59. Somsen, B. A. *et al.* Functional mapping of the 14-3-3 hub protein as a guide to design 14-3-3 molecular glues. *Chem Sci* **13**, 13122–13131 (2022).
60. Vonrhein, C. *et al.* Data processing and analysis with the autoPROC toolbox. *Acta Crystallogr D Biol Crystallogr* **67**, 293–302 (2011).
61. Potterton, L. *et al.* CCP4i2: the new graphical user interface to the CCP4 program suite. *Acta Crystallogr D Struct Biol* **74**, 68–84 (2018).
62. Evans, P. R. An introduction to data reduction: space-group determination, scaling and intensity statistics. *Acta Crystallogr D Biol Crystallogr* **67**, 282–292 (2011).
63. Evans, P. R. & Murshudov, G. N. How good are my data and what is the resolution? *urn:issn:0907-4449* **69**, 1204–1214 (2013).
64. Vagin, A. & Teplyakov, A. Molecular replacement with MOLREP. *urn:issn:0907-4449* **66**, 22–25 (2009).
65. Lebedev, A. A., Vagin, A. A. & Murshudov, G. N. Model preparation in MOLREP and examples of model improvement using X-ray data. *urn:issn:0907-4449* **64**, 33–39 (2007).
66. Murshudov, G. N. *et al.* REFMAC5 for the refinement of macromolecular crystal structures. *Acta Crystallogr D Biol Crystallogr* **67**, 355–367 (2011).
67. Kovalevskiy, O., Nicholls, R. A., Long, F., Carlon, A. & Murshudov, G. N. Overview of refinement procedures within REFMAC 5: Utilizing data from different sources. *Acta Crystallogr D Struct Biol* **74**, 215–227 (2018).
68. Emsley, P., Lohkamp, B., Scott, W. G. & Cowtan, K. Features and development of Coot. *Acta Crystallogr D Biol Crystallogr* **66**, 486–501 (2010).

579 **Methods**
580
581 **Protein purification and peptide synthesis**
582 Recombinant human full-length Tau (2N4R, hTau40) and Tau$^{\Delta K280}$ were expressed in *E. coli*
583 BL21 Star (DE3) (Invitrogen) cells as previously described [58] and purified following an
584 established protocol [34]. 14-3-3 protein zeta (14-3-3ζ) and 14-3-3 protein zeta truncated after
585 T234 (14-3-3ζΔC, for crystallography) were expressed in NiCo21 (DE3) competent cells and
586 purified as previously described following an established protocol [59]. All recombinant purified
587 and further modified proteins were stored aliquoted at −80°C.
588
589 **Tau peptides**
590 Acetylated and fluorescein (FITC)-labeled tau peptides for crystallography and fluorescence
591 anisotropy were purchased from GenScript (sequence:
592 SRTP{pSER}LPTPPTREGGGSGGGSGGGVTSKCG{pSER}LGNIHHK).
593
594 **14-3-3ζ X-ray crystallography data collection, analysis, and refinement binary structure**
595 The 14-3-3ζΔC protein and the acetylated Tau$^{pS214/pS324}$ peptide were dissolved in
596 complexation buffer (20 mM HEPES pH 7.5, 2 mM MgCl2 and 100 μM TCEP) and mixed in a
597 1:1 molar stoichiometry (protein:peptide) at a final protein concentration of 15 mg/ml. The
598 complex was set up for sitting-drop crystallization and crystals were grown within one month
599 at 4°C in 0.2M Sodium Fluoride, 0.1M bis-tris propane pH 6.5, 20% w/v PEG 3350. Crystals
600 were fished and flash-cooled in liquid nitrogen. X-ray diffraction (XRD) data was collected at
601 the European Synchrotron Radiation Facility (ESRF) beamline ID23-1, Grenoble, France.
602 autoPROC software (version 1.1.7) was used to index and integrate the diffraction data [60]. The
603 data was further processed using the CCP4i2 suite (version 8.0.002) [61]. Scaling was performed
604 using AIMLESS [62,63]. MolRep [64,65] was used for phasing, using PDB ID 5D2D as template.
605 REFMAC (version 5) [66,67] was used for initial structure refinement. Correct peptide sequences
606 were modelled in the electron density in COOT (version 0.9.8.1) [68]. Alternating cycles of model
607 improvement and refinement were performed using COOT and REFMAC. Figures were
608 generated with PyMOL (version 2.5.2). 2Fo-Fc electron density maps were contoured at 1σ.
609 See Table S and for XRD data collection, structure determination, and refinement statistics.
610 The structures were submitted to the PDB with IDs: 8QDV. Code availability: All code used to
611 analyze data has been previously published.
612
613 ***In vitro* phosphorylation of Tau**
614 Tau protein (6-8 mg/ml) was incubated in phosphorylation buffer (25 mM HEPES, 100 mM
615 NaCl, 5 mg MgCl, 2 mM EGTA, 1 mM DTT, Protease Inhibitors) with recombinant PKA kinase
616 (2500 U/mg, NEB-P600S) and 1 mM ATP overnight at 30°C and 250 rpm. To denature and
617 remove the kinase from the sample, NaCl was added to a final concentration of 500 mM. The
618 protein solution was boiled for 10 min at 95 °C, and spun at 100000 g for 40 min. The
619 phosphorylated Tau in the supernatant was dialyzed against phosphate buffered saline (PBS)
620 containing 1 mM DTT, or against 25 mM HEPES, 10mM NaCl, 1 mM DTT, pH 7.4 for LLPS
621 assays.
622
623 **Fluorescence anisotropy assay (FA)**
624 14-3-3ζ was titrated in a 2-fold dilution series (starting at 400 μM 14-3-3ζ) to 10 nM of
625 fluorescein labeled peptide (Tau^{pS214}, Tau^{pS324}, Tau$^{pS214/pS324}$) in FA buffer (10 mM HEPES pH

626 7.4, 150 mM NaCl, 50 µM TCEP, 0.1% (v/v) Tween20, 0.1% (w/v) BSA). Dilution series were
627 made in polystyrene low-volume 384-well plates (Corning #4514, Black Round Bottom).
628 Measurements were performed directly after plate preparation, using a Tecan SPARK plate
629 reader at room temperature (λ_{ex}: 485±20 nm; λ_{em}: 535±25 nm; mirror: automatic; flashes: 30;
630 settle time: 1 ms; gain: optimal; Z-position: calculated from well). Wells containing only
631 fluorescein labelled peptide were used to set as G-factor calibrated from these wells. All data
632 were analyzed using GraphPad Prism (10.0.1) and fitted with a four-parameter logistic model
633 (4PL) to determine binding affinities (dissociation constant, KD). All results are based on three
634 independent experiments from which the average and standard deviations for each KD were
635 determined using excel. Tau competition assays were performed in a similar way but using
636 full-length Tau constructs (WT, PKA-WT, PKA-Tau^{S214A}, PKA-Tau^{S324A}, PKA-Tau$^{S214A/S324A}$)
637 titrated in a 2-fold dilution series (starting from 50 µM) to 1 µM 14-3-3ζ and 10 nM fluorescein
638 labelled Tau$^{pS214/pS324}$ peptide.
639
640 **Differential Scanning Fluorimetry (DSF)**
641 DSF was performed using 40 µl samples containing 2.5 µM 14-3-3ζ and 25 µM tau and 5x
642 ProteoOrange (Lumiprobe, 5000x stock in DMSO) in 10 mM HEPES, 150 mM NaCl, 50 µM
643 TCEP (pH 7.4). The samples were heated from 35 °C to 79°C at a rate of 0.3 °C per 15 s in a
644 CFX96 Touch Real-Time PCR Detection System (Bio-Rad). Fluorescence intensity was
645 determined using excitation (λ_{em}=525/20 nm) and emission (λ_{ex}=570/20 nm) filters. Based on
646 these melting curves, the negative derivative melting curve is obtained from which the melting
647 temperature Tm was determined. ΔTm values represent the differences in melting temperature
648 relative to the 14-3-3ζ control. All described melting temperatures are based on three
649 independent experiments, from which the average and standard deviations were determined.
650
651 **Fluorescent labeling of Tau and 14-3-3ζ**
652 Fluorescent labelling of Tau and 14-3-3ζ protein for microscopy assays was done using amine-
653 reactive DyLight405 or DyLight488-NHS ester (Thermo Scientific) following the manufacturer
654 instructions and the established protocol [34].
655
656 **Condensate formation and fluorescence microscopy**
657 Prior to condensation assays, all proteins used were dialyzed against 25 mM HEPES, 10 mM
658 NaCl, 1 mM DTT, pH7.4 and stored at -80°C. LLPS of Tau (10 µM, 2% DyLight488-Tau) with
659 14-3-3ζ (1-20 µM, 2% DyLight650-14-3-3z) variants was performed in 25 mM HEPES, 1 mM
660 DTT, pH7.4 buffer (final NaCl concentration in sample 1-5 mM) in the presence of 5 % (w/vol)
661 PEG-8000, except otherwise indicated. Directly after LLPS induction, 2-3 µl sample were
662 pipetted onto a amine-treated glass-bottom dish for imaging (TC-treated Miltenyi CG 1.5,
663 diameter = 3.5 mm). Imaging dishes were immediately closed and equipped with a ddH_2O-
664 soaked paper tissue lining the inner edges to avoid evaporation of the LLPS sample. Imaging
665 was performed 1 h after droplet formation either on a widefield epifluorescence microscope
666 (Ti2, Nikon) or a spinning disk confocal microscope (CSU-X, Nikon) equipped with 40x air or
667 60x oil objective, respectively.
668
669 **Western Blot**
670 Tau variants (0.5 µg protein) and neuronal lysates (10 µg protein), was separated by SDS-
671 PAGE (NuPage 4-12% Bis-Tris, Invitrogen) and blotted onto a nitrocellulose membrane. The
672 membrane was blocked with 3% BSA in PBS containing 0.05% Tween (PBS-T) at room
673 temperature for 1 h, followed by the incubation with primary anti-phospho-Tau antibodies

674 (rabbit anti-pS214 Tau, Abcam, ab170892 (1:1000); rabbit anti-pS324 Tau, Abcam, ab109401
675 (1:5000)) or and anti-total Tau antibody (rabbit anti-human Tau, Dako, #A0024 (1:5,000))
676 diluted in 3% BSA in PBS-T overnight at 4°C shaking. After washing with PBS-T, the
677 membrane was incubated with HRP-conjugated secondary antibody (goat anti-rabbit HRP,
678 BioLabs 7074P2) in 3% BSA in PBS-T shaking for 1-2 h at room temperature, washed in PBS-
679 T, and then developed using a chemiluminescent substrate (LumiGLO, Peroxide, 7003, Cell
680 Signaling) and an imaging device (Fusion Fx7).
681
682 **Fluorescence recovery after photobleaching (FRAP)**
683 Condensates (containing 2%Tau-DyLight488 and 2%14-3-3ζ-DyLight650) were imaged in a
684 triggered acquisition mode before and directly after bleaching for 40 sec (round ROIs, cross
685 sections 1-2 μM) with a 650 nm laser, followed by a 488 nm laser (90% intensity; 3 loops). In
686 each field of view, same-sized background ROI (outside condensates) and non-bleached
687 reference-ROI (inside different condensates) were measured. All FRAP measurements were
688 background corrected and normalized to the background corrected reference signal. FRAP
689 experiments were performed on a spinning disk confocal microscope (CSU-X, Nikon) using a
690 60x oil objective.
691
692 **Primary neuron assay**
693 All animal procedures were performed in agreement with the German animal welfare act and
694 have been approved by the Berlin State Office for Health and Social Affairs (LaGeSo).
695 Primary hippocampal mouse neurons were prepared from dissected hippocampi of postnatal
696 (P0-1) wild-type mice and grown under standard conditions in PDL-coated 8-well imaging
697 dishes (ibidi). On DIV5, neurons were AAV transduced for the expression of EGFP-tagged
698 mutant Tau (pAAV.CAG.EGFP-Tau$^{P301L/S320F}$). Neurons were treated with BV02 (10 µM or 40
699 µM; #SML0140, Sigma) or Fusicoccin (50 µM; # sc-200754, Santa Cruz) on DIV8 for 48 h. On
700 DIV10, neurons were fixed in 4% PFA in PBS, counterstained with DAPI for 10 min, and
701 imaged on a Nikon scanning Confocal A1Rsi+ microscope. A 10x air objective was use to
702 acquire images of a large field of view (entire well of culture dish) for quantification, and a 60x
703 oil objective to collect images of individual neurons.
704
705 **Thioflavine-T Tau aggregation assay**
706 Tau (10 μM Tau$^{\Delta K280}$ and PKA-Tau$^{\Delta K280}$) aggregation in the presence and absence of 14-3-
707 3ζ (20 μM) was induced by adding heparin (0.115 mg/ml, MW = 8–25 kDa (~7 μM), Applichem)
708 in PBS, pH7.4, 1 mM DTT. Thioflavin-T (ThioT, 50 μM, Sigma) was added to detect the
709 aggregation. Samples were prepared in triplicates, pipetted into black clear-bottom 384-well
710 μClear plates (Greiner), and ThioT fluorescence (λ_{Ex} = 440 nm, λ_{Em} = 485 nm) was recorded in
711 a plate reader (Infinite M Plex, Tecan) following a 5 sec shake every 15 min at 37°C.
712
713 **Microtubule pelleting assay**
714 To assess the binding of Tau to MTs, we used a MT binding protein spin-down assay kit (#
715 BK029, Cytoskeleton, Inc.) according to the manufacturer's instructions. Briefly, MTs were
716 assembled from soluble tubulin in MT assembly buffer (80 mM PIPES pH 7.0, 2 mM MgCl2,
717 0.5 mM EGTA) at 35°C for 20 min and stabilized with Taxol, yielding a concentration of
718 approximately $5x10^{11}$ MT/ml. For MT binding, 0.4 μg recombinant Tau (Tau or PKA-Tau) with
719 or without 1 μg 14-3-3ζ were incubated with 20 μl preformed MTs for 30 min. Prepared
720 reactions (50 μl) were carefully added on top 100 μl cushion buffer (80 mM PIPES pH 7.0, 1
721 mM MgCl2, 1 mM EGTA, 60% glycerol) in small ultracentrifuge tubes (#343775, Beckmann)

722 and centrifuged at 100000 g at room temperature for 40 min. After centrifugation, supernatant
723 (50 μl) and pellet were separated and SDS sample buffer was added. Samples were analyzed
724 by SDS-PAGE and western blot using total human Tau (#835201, Biolegend), 14-3-3
725 (#ab51129, Abcam), and α-tubulin (#T6074, Sigma) antibodies.
726
727 ***In vitro* microtubule bundle formation**
728 Bovine tubulin (5 μM total tubulin, 10% Alexa594-labeled tubulin (PUR-032005 and PUR-
729 059405, PurSolutions):) and 1 mM GTP in freshly prepared and filtered polymerization buffer
730 (BRB80, 1 mM DTT, pH 6.8) were added to Tau (25 μM; 2% DyLight488-Tau) with and without
731 14-3-3ζ (12.5 μM; 2% DyLight650-14-3-3ζ) and in the presence of 5% (w/vol) PEG8000.
732 Samples were pipetted into multi-well glass bottom dishes (μ-Slide Angiogenesis glass bottom
733 dishes, Ibidi), and MT bundles, Tau, and 14-3-3ζ were imaged using a confocal spinning disc
734 microscope (CSU-X, Nikon) with a 60x oil objective.
735
736 **Data analysis and presentation**
737 Data have been statistically analyzed using Graphpad Prism10 and the therein provided
738 algorithms. Data presentation was done in Graphpad Prism 10 as well. Model containing figure
739 panels were created (in part) using Biorender.
740
741 **Data availability**
742 Raw data for imaging, western blots, and FRAP are available upon request. Crystal structures
743 are deposited on PDB (ID: 8QDV).
744
745 **Material availability**
746 Protein expression plasmids are available upon request or available from Addgene. The amino
747 acid sequence of the Tau phospho-peptide pS2 is provided to enable independent synthesis.
748
749 **Inclusion and Ethics**
750 All individuals that contributed to research, manuscript writing, and the reviewing process have
751 been included in the author list and asked for their consent with the order in the author list and
752 the content of eth manuscript.
753
754 **Contributions**
755 J.H., performed *in vitro* LLPS and aggregation, FRAP, and MT imaging experiments, drafted
756 initial Figures and helped writing the manuscript. M.C.M.v.d.O, determined crystal structure of
757 14-3-3ζ in complex with pS2, performed fluorescence anisotropy and thermal stability
758 measurements, helped writing the manuscript. L.D., performed neuron experiments and MT
759 pelleting assay, and helped reviewing the manuscript. L.L, helped with LLPS experiments and
760 designed 14-3-3ζ mutant. R.P. and M.F. helped with cell experiments. E.S., cloned and
761 generated mutant Tau AAV. S.M. helped with data analysis and reviewing the manuscript.
762 C.O., helped supervising experiments, provided funding, reviewed manuscript. L.B., designed
763 study, provided funding, supervised team at University Eindhoven, reviewed manuscript. S.W.,
764 designed study, provided funding, supervised team at DZNE Berlin, wrote and reviewed
765 manuscript.
766
767 **Acknowledgements**
768 We thank Michelle Arkin (UCSF) for stimulating discussions. The crystallography data
769 collection was performed at the European Synchrotron Radiation Facility (ESRF), Grenoble,

France. We would like to thank Lindsay McGregor for assistance in using beamline ID23-1. Beamtime was allocated for proposal MX-2407 (doi 10.15151/ESRF-ES-1006014569).

Funding

S.W. received funding form the German Research Foundation (DFG) in the priority program SPP2191 (project 419138680), the Hertie Foundation (project P1200002), the Alzheimer Association (AARG-22_972303), and the DZNE in the Helmholtz Society.
L.B. received funding from the European Union through ERC Advanced Grant PPI-Glue (101098234) and the Netherlands Ministry of Education, Culture and Science (Gravity program 024.001.035). Views and opinions expressed are however those of the authors only and do not necessarily reflect those of the European Union or the European Research Council. Neither the European Union nor the granting authority can be held responsible for them.
C.O. received funding from The Netherlands Organization for Scientific Research (NWO) through OCENW.KLEIN.300_10393.

Conflict of Interest

Christian Ottman and Luc Brunsveld are both co-founders of Ambagon Therapeutics. Christian Ottmann is currently employee and Luc Brunsveld is currently advisor of Ambagon Therapeutics.

Figures

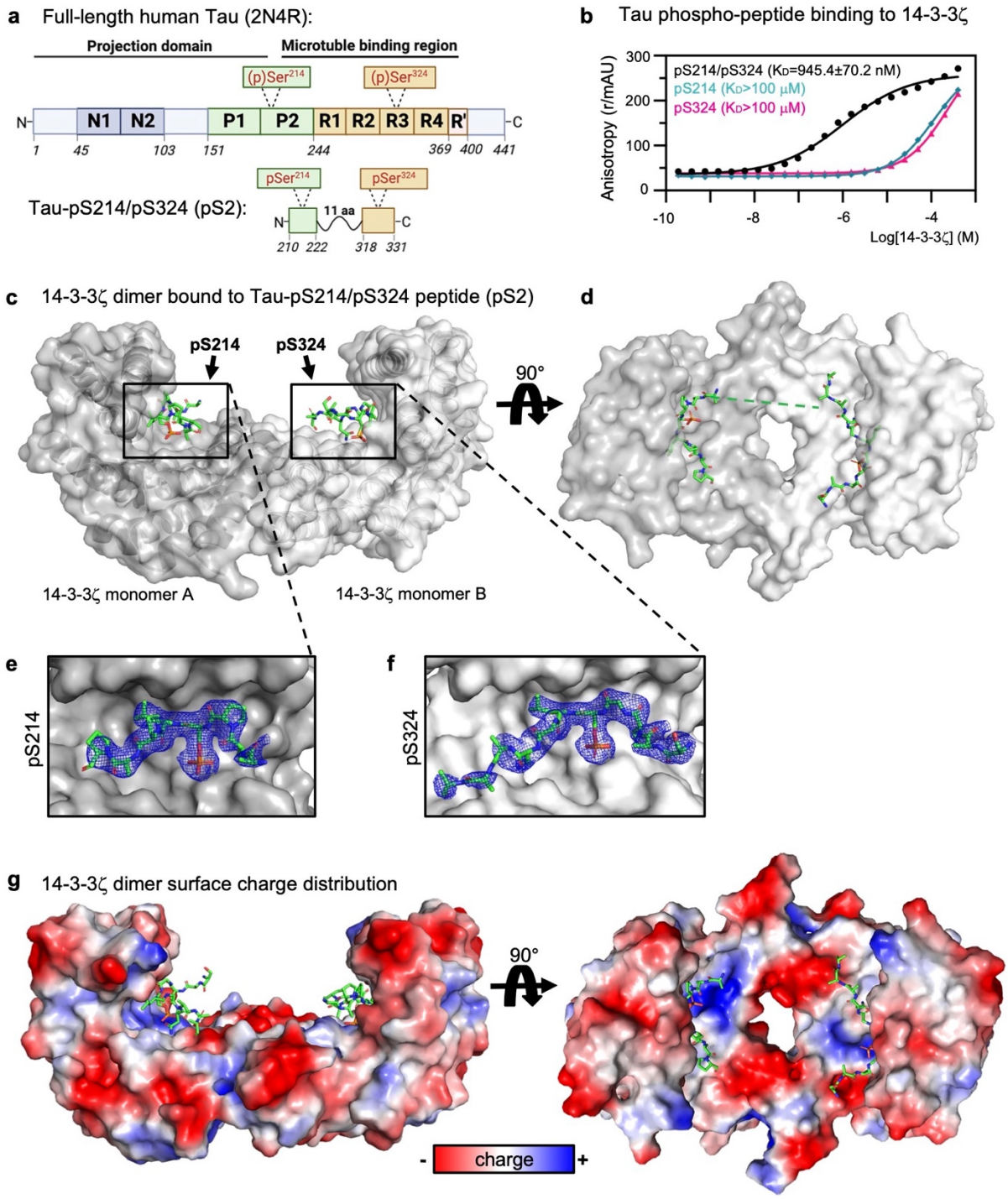

Figure 1. Crystal structure of 14-3-3ζ dimer in complex with the peptide Tau-pS214/pS324.

a, Domain structure of the longest human Tau isoform (2N4R, 441 aa) consisting of the N-terminal projection domain with two N-terminal inserts (N1, N2), the proline-rich domain (P1+P2), and the C-terminal microtubule binding region that includes four pseudo-repeats (R1-R4) and short sequences up- and downstream of these. Phosphorylation of serine residues S214 and S324 enables 14-3-3ζ binding to Tau. Domain structure of phospho-peptide Tau-pS214/pS324 (pS2) is shown as well (38aa; Tau$^{210\text{-}222(pS214)}$-GGGSGGGSGGG-Tau$^{318\text{-}331(pS324)}$.

b, Fluorescent anisotropy measurements for the binding of Tau-pS214/pS324, Tau-pS14, and

Tau-pS324 peptides to 14-3-3ζ. 14-3-3ζ was titrated into 10 nM of respective fluorescein-labeled Tau peptide. Data shown as mean±SD, representative experiment with N=3 technical replicates (see Extended Data Fig S1 for two more experiments). **c,** Cartoon showing semi-transparent surface of the 14-3-3ζ dimer (gray) complexed with the pS214 and pS324 binding sites of the tau peptide (green rods). **d,** Top view of pS214 and pS324 binding sites (green rods) into the 14-3-3ζ binding grooves (grey semi-transparent surface). Green dash line shows connective amino acid residues between the binding sites. **e+f,** Close-up of the binding grooves of monomer A and B (grey surface) containing the tau peptide binding sites (green rods). Final 2Fo-Fc electron density map of the peptide is shown (blue mesh, contoured at 1s). **g,** Surface charge distribution on 14-3-3 ζ dimers mapped on the crystal structure shown in e and f. Negatively charged areas are indicated in red, and positively charged ones in blue. Note that the binding pocket of the Tau phospho-peptide, pS2, is positively charged, whereas much of the outer surface of 14-3-3ζ is negatively charged.

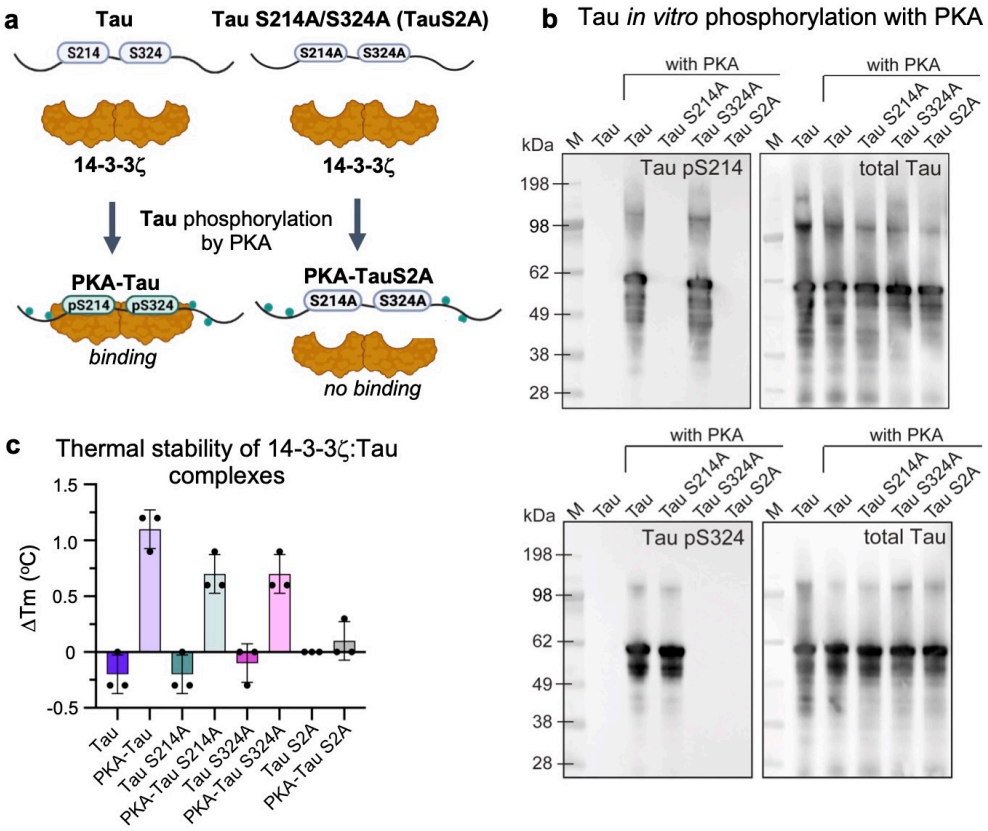

Figure 2. Binding of 14-3-3ζ depends on Tau phosphorylation at Ser214 and Ser324. **a,** Schematic: Full-length Tau binding to 14-3-3ζ depends on phosphorylation at serine residues S214 and S324. **b,** Western blots of recombinant Tau variants *in vitro* phosphorylated using PKA kinase (Tau variants: wildtype Tau, Tau S214A, Tau S324A, Tau S214A-S324A (Tau S2A)) using antibodies specific for phosphorylated residues in Tau (Tau pS214 and Tau pS324) and total Tau. **c,** Thermal shift assay of PKA-phosphorylated and non-phosphorylated Tau variants binding to 14-3-3ζ. PKA-phosphorylation significantly increases binding of Tau to 14-3-3ζ, which is reduced upon S>A mutation of the relevant phosphorylation sites, S214A and S324A. Mutation of both serine residues abolishes Tau binding. Data shown as mean±SD, N=3 independent experiments. One-way ANOVA with Tukey post-test.

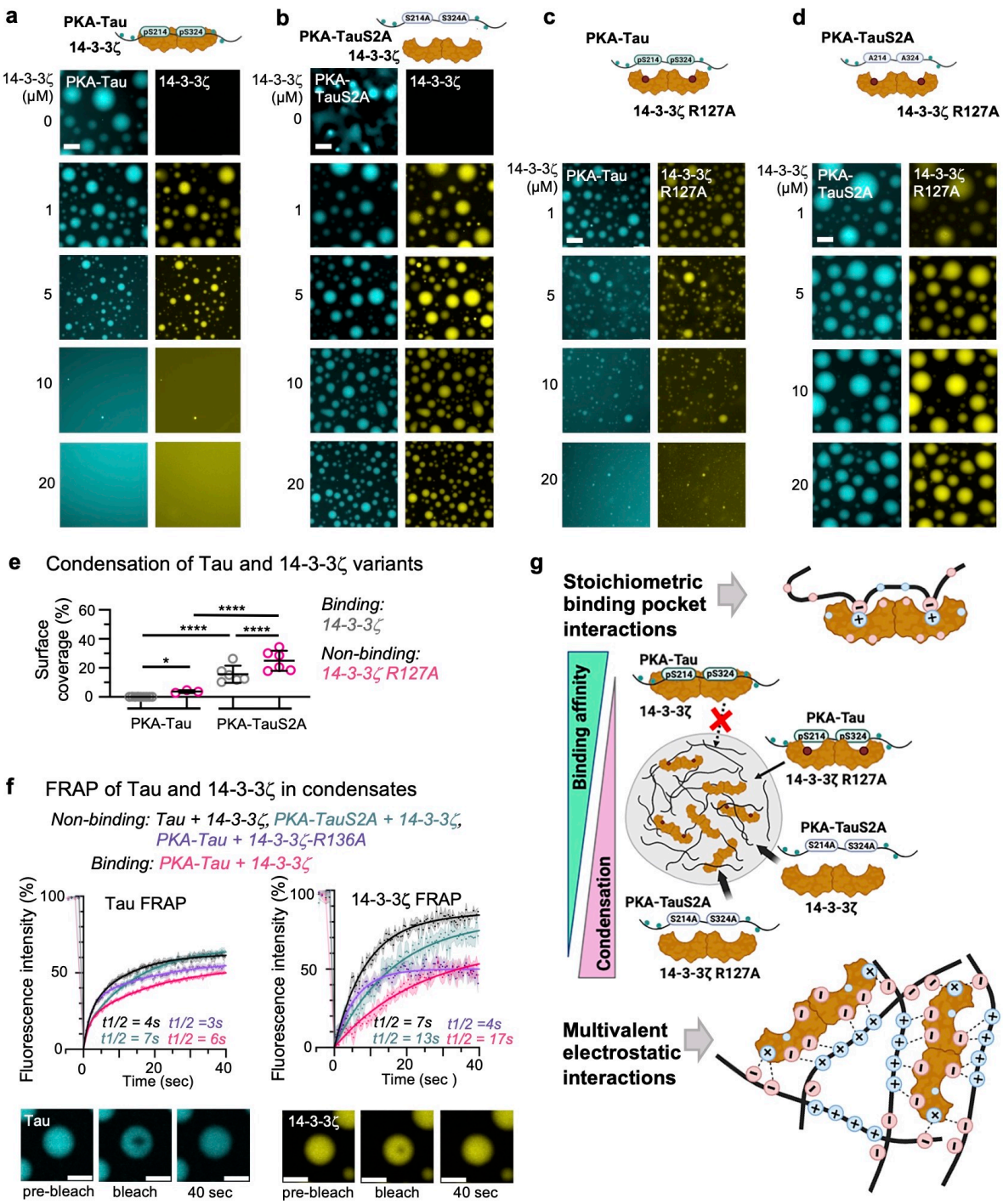

Figure 3. Stoichiometric binding of 14-3-3ζ inhibits Tau condensation.

a+b, Representative fluorescence microscopy images of 10 μM PKA-Tau (A), and PKA-TauS2A (B) with increasing 14-3-3ζ concentrations (0, 1, 5, 10, 20 μM) in 25 mM HEPES, 1 mM DTT, pH 7.4 buffer in the presence of 5% (w/v) PEG. 2% Tau labeled with DyLight488, 2% 14-3-3ζ labeled with DyLight647. Scale bars = 20 μM. **c+d,** Representative images of 10 μM PKA-Tau (C), and PKA-TauS2A (D) with increasing 14-3-3ζ R127A concentrations (1, 5, 10, 20 μM) in 25 mM HEPES, 1 mM DTT, pH 7.4 in the presence of 5% PEG. Scale bars = 20 μm. **e,** Quantification of condensate surface coverage (%) of 10 μM PKA-Tau and PKA-TauS2A with 10 μM 14-3-3ζ (grey) or 14-3-3ζ R127A (pink) in 25 mM HEPES, 1 mM DTT, pH 7.4 in the presence of 5% PEG. All PKA-Tau variants mixed with the non-binding mutant 14-3-3ζ R127A show more condensation. Data shown as mean±SD. One-way ANOVA with

841 Tukey post-test. Data points represent individual analyzed images, three images per
842 condition, 1-3 experimental replicates. **f,** FRAP of PKA-Tau, PKA-TauS2A, and Tau (10 μM,
843 2% DyLight488-labeled Tau) with 14-3-3ζ or 14-3-3ζ R127A (5 μM, 2% DyLight650-labeled
844 14-3-3ζ). Data presented as mean±SEM; N=9-20 condensates per condition. Solid lines show
845 double exponential fit to the data (circles), fit data shown in Supplemental Figure S1. $t_{1/2}$ = time
846 to half recovery. Scale bars of representative FRAP images = 5 μm. **g,** Model: The
847 stoichiometric binding of Tau to 14-3-3ζ dimers correlates inversely with Tau:14-3-3ζ co-
848 condensation, which is driven by multivalent electrostatic interactions. PKA-Tau and 14-3-3ζ
849 have the highest binding affinity and show no co-condensation at equimolar concentrations
850 (10 μM Tau, 10 μM 14-3-3ζ), whereas PKA-TauS2A with 14-3-3ζ R127A has a low binding
851 affinity and shows the strongest co-condensation.
852
853

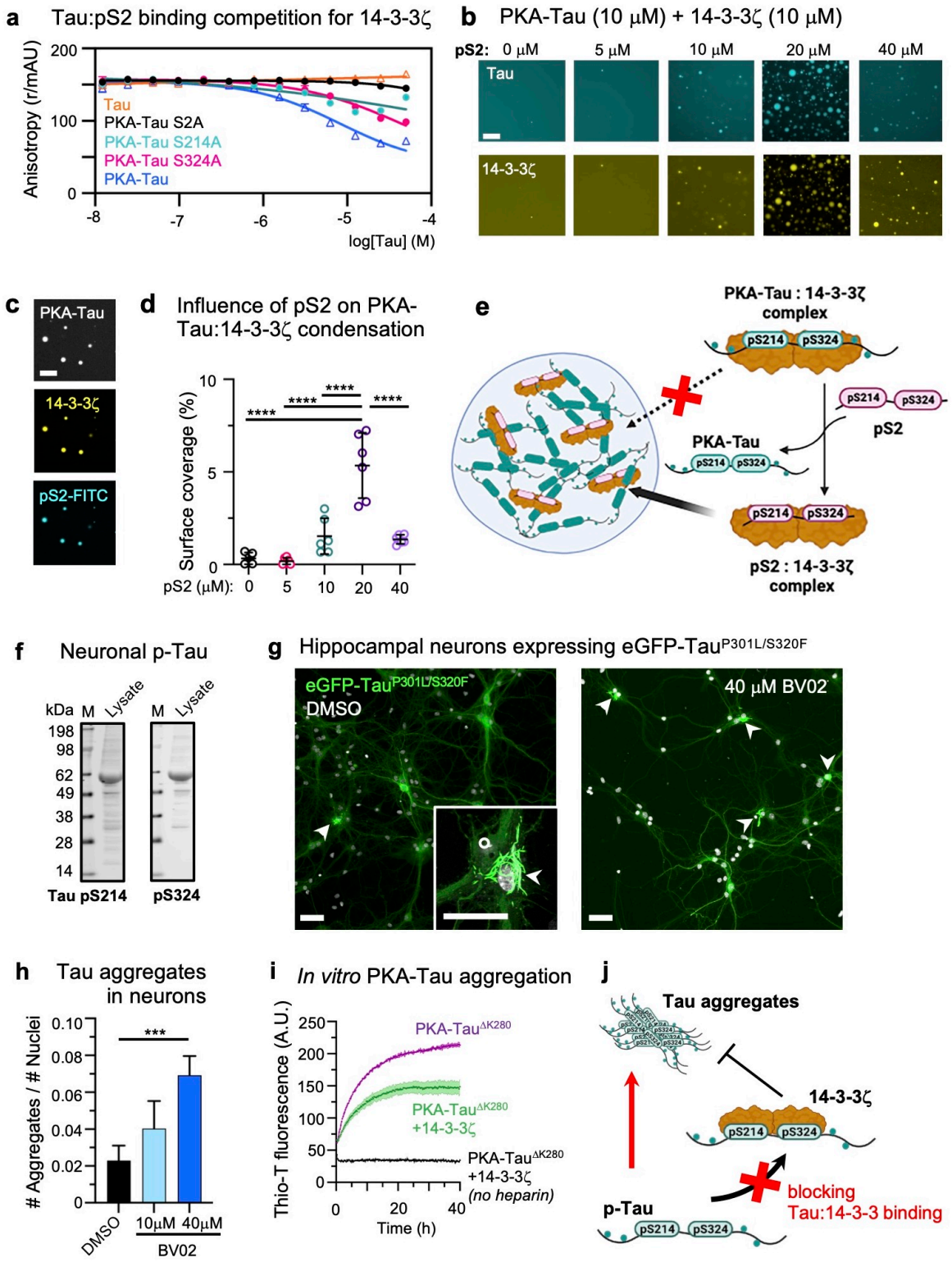

Figure 4. Phospho-Tau peptide pS2 competes with PKA-Tau for 14-3-3ζ binding. **a,** Model for pS2 competition with PKA-Tau for the binding to 14-3-3ζ. **b,** Fluorescent anisotropy measurements for the competition between phospho-Tau variants and fluorescein-labeled pS2 peptide (pS2-FITC) for the binding to 14-3-3ζ (1 μM). Tau variants were titrated into a solution of 10 nM fluorescein-labeled pS2 and 1 μM 14-3-3ζ. Data shown as mean±SD, representative experiment with N=3 technical replicates (see Extended Data Fig S6 for other two experiments). **c,** Representative images of PKA-Tau (10 μM) with 14-3-3ζ (10 μM) and

863 increasing concentrations of the pS2 (0, 5, 10, 20, 40 μM) in 25 mM HEPES, 1 mM DTT,
864 pH 7.4 buffer in the presence of 5% PEG. Scale bars = 20 μM. **d,** Quantification of condensate
865 surface coverage (%) for PKA-Tau with 14-3-3ζ and pS2. Data shown as mean±SD. One-way
866 ANOVA with Tukey post-test. Data points represent individual analyzed images, three images
867 per condition, 2 experimental replicates. **e,** Representative images of PKA-Tau (10 μM,
868 including 2% DyLight405-labeled PKA-Tau) with 14-3-3ζ (10 μM, including 2% DyLight650-
869 labeled 14-3-3ζ) and pS2 (20 μM, including 2% FITC-pS2) in 25 mM HEPES, 1 mM DTT,
870 pH7.4 buffer in the presence of 5% PEG. Scale bars = 10 μM. **f,** Inhibition of soluble p-Tau
871 aggregation through complexation by 14-3-3ζ dimers. **g,** Western blots of cell lysates from
872 cultured primary mouse neurons show phosphorylation of endogenous mouse Tau at S214
873 and S324. **i,** Representative images of primary hippocampal neurons (DIV12) transduced with
874 AAV to express aggregating FTD-mutant eGFP-Tau$^{P301L/S320}$. Neurons were treated with
875 DMSO (control) or BV02 (40 μM) for 48h, starting 3 days after AAV transduction. Inset shows
876 fibrillar aggregates formed in a subset of neurons expressing eGFP-Tau$^{P301L/S320}$. White arrow
877 heads indicate neurons with aggregates in the soma, white circle a neighboring neuron without
878 Tau aggregation. Scale bar = 20 μM. **h,** Quantification of Tau aggregates in neurons upon
879 treatment with DMSO or BV02 (10 or 40 μM). Data shown as mean±SD, N=4 analyzed images,
880 one-way ANOVA with Tukey post-test. **i,** Thioflavine-T (Thio-T) assay of pro-aggregant FTD-
881 mutant Tau and PKA-Tau (DK280 mutation) aggregation (triggered with heparin) in the
882 absence and presence of 14-3-3ζ. N=3 replicates. Data shown as mean±SD normalized to
883 Tau$^{\Delta K280}$ or PKA-Tau$^{\Delta K280}$ without 14-3-3ζ. **j,** Model: Binding of 14-3-3ζ to Tau phosphorylated
884 at residues S214 und S324 promotes its solubility and thereby prevents its aggregation.
885 Blocking the interaction (red cross), e.g., by BV02, in turn promotes Tau aggregation (red
886 arrow).
887
888

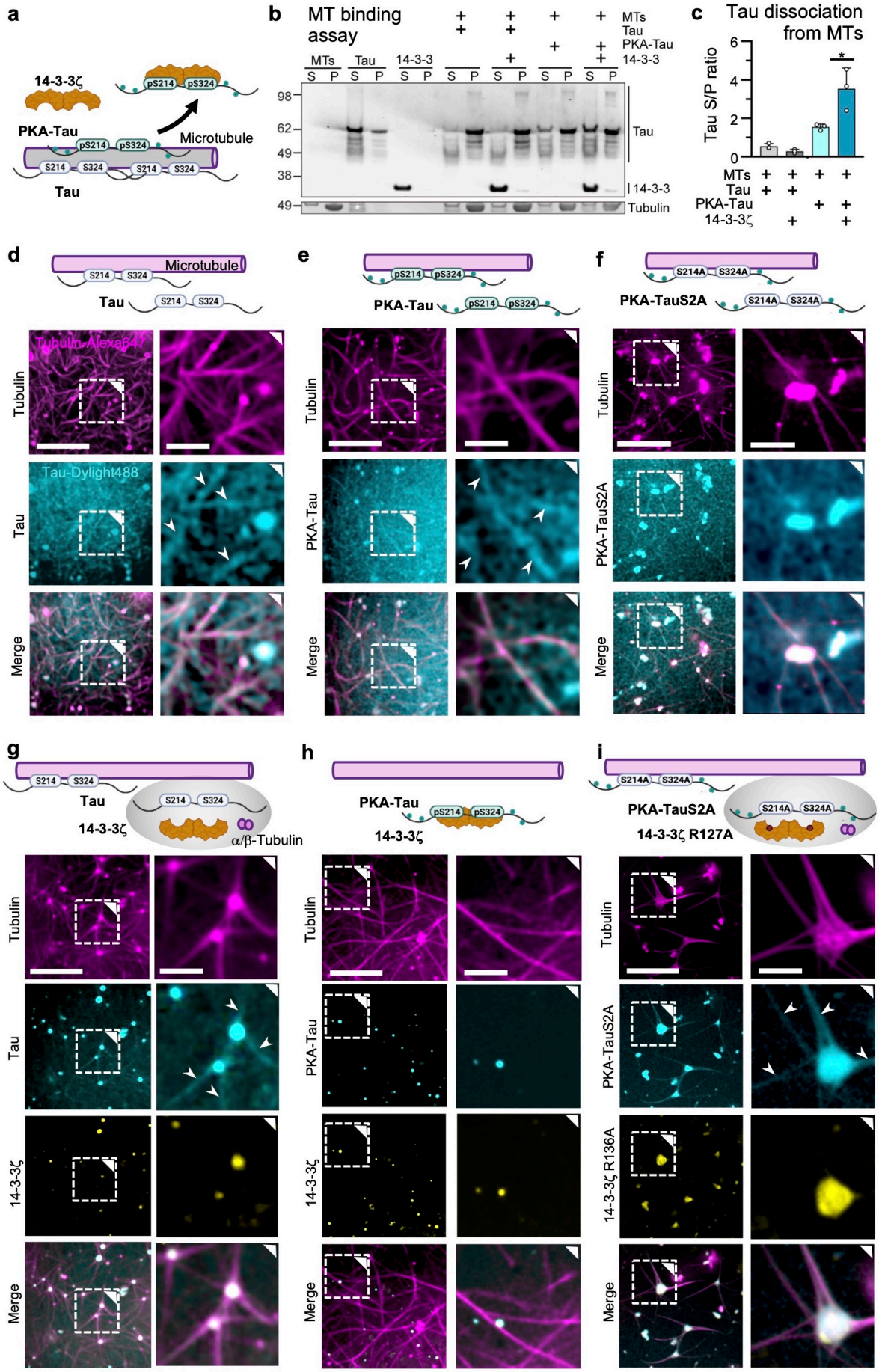
a
14-3-3ζ
pS214
pS324
PKA-Tau
Microtubule
S214
S324
Tau
b
MT binding assay
MTs
Tau
PKA-Tau
14-3-3
S P
98
62
49
38
49
Tau
14-3-3
Tubulin
c
Tau dissociation from MTs
Tau S/P ratio
6
4
2
0
MTs
Tau
PKA-Tau
14-3-3ζ
d
Microtubule
Tau
Tubulin-Alexa647
Tubulin
Tau-Dylight488
Tau
Merge
e
PKA-Tau
PKA-Tau
f
S214A
S324A
PKA-TauS2A
PKA-TauS2A
g
14-3-3ζ
α/β-Tubulin
14-3-3ζ
h
i
14-3-3ζ R127A
14-3-3ζ R136A

889

Figure 5. 14-3-3ζ promotes phospho-Tau dissociation from microtubules.
a, Model for 14-3-3ζ promoting phospho-Tau detachment from MTs. **b,** Western blot of MT binding assay for Tau and PKA-Tau with and without 14-3-3ζ. **c,** Supernatant (soluble unbound) to pellet (MT bound) S/P ratio of Tau and PKA-Tau. Quantification of MT binding assay. Data shown as mean±SD, N=3 independent assays, One-way ANOVA with Tukey post-test. **d,e,f,** Confocal images of *in vitro* MT formation with Tau variants (25 μM, 5% PEG) show Tau coating of MTs and remaining soluble Tau in solution: un-phosphorylated Tau **(d)**, PKA-Tau **(e)**, and PKA-TauS2A **(f)**. Scale bars = 20 μm, and 5 μm in zoomed insets. **g,h,i,** Images of MT formation with Tau (25 μM, 5% PEG) and 14-3-3ζ (12.5 μM). When 14-3-3ζ does not bind Tau (Tau+14-3-3ζ **(g)** and PKA-TauS2A+14-3-3ζ **(i)**), Tau coats MTs, no free Tau is in solution, and MTs grow from condensates containing Tau, 14-3-3ζ, and tubulin (=MT asters). When 14-3-3ζ is binding Tau (PKA-Tau+14-3-3ζ **(h)**), phospho-Tau is absent on MTs and few Tau:14-3-3ζ condensates form in solution, not attached to MTs. Scale bars = 20 μm, 5 μm in zoomed insets.

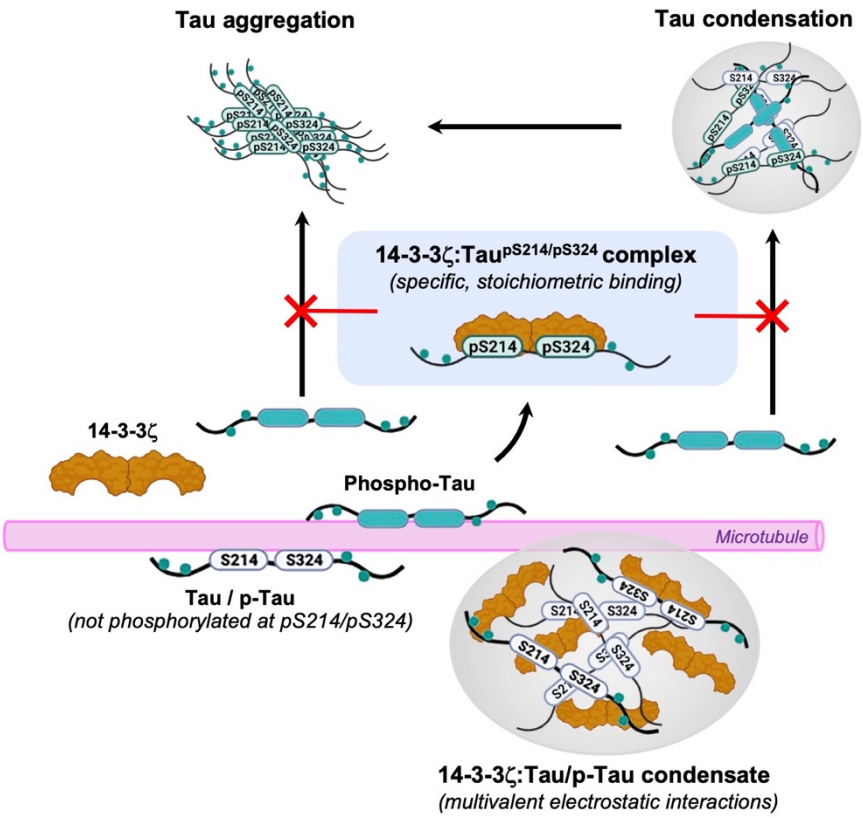

Figure 6. Regulation of Tau MT binding, condensation, and aggregation by 14-3-3ζ. 14-3-3ζ dimers form stable stoichiometric complexes with Tau$^{pS214/pS324}$. This enables the efficient dissociation of Tau$^{pS214/pS324}$ from MTs, which may contribute to ensure MT dynamics. In addition, the formation of 14-3-3ζ:Tau$^{pS214/pS324}$ complexes prevents the aggregation of Tau in the cytosol by inhibiting p-Tau assembly into fibrillar aggregates and/or liquid-like condensates. In non-binding conditions, when Tau is not phosphorylated at S214 and S324, 14-3-3ζ co-condenses with Tau based on multivalent electrostatic interactions. These condensates attach to MTs, when present, and sequesters excess Tau from the solution. Whether 14-3-3ζ:Tau condensates have of cellular function remains to be clarified.

920 **Extended Data Figures**

921

a

Tau_pS214_pS324 (**pS2**)	SRTP(pS)LPTPPTREGGGSGGGSGGGVTSKCG(pS)LGNIHHK
Tau_pS214	SRTP(pS)LPTPPTRE
Tau_pS324	VTSKCG(pS)LGNIHHK

b

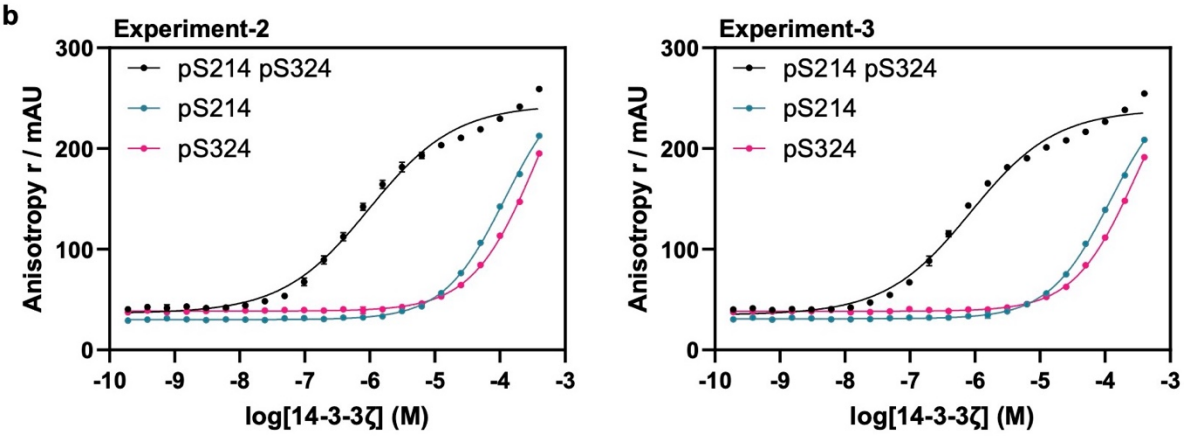

922

923

924 **Extended Data Figure S1. Anisotropy of Tau phospho-peptide binding to 14-3-3ζ.**
925 **a,** Amino acid sequences (letter code) of Tau phospho-peptides used for anisotropy
926 measurements. Single phospho-site Tau peptides: Tau_pS14 and Tau_pS324. Double
927 phospho-site peptide: $Tau^{pS214/pS324}$ (pS2; 38aa; $Tau^{210\text{-}222(pS214)}$-GGGSGGGSGGG-$Tau^{318\text{-}}$
928 $^{331(pS324)}$. Phospho-sites are marked in red letters, linker region in blue letters. **b,** Independent
929 experimental replicates of fluorescence anisotropy measurements for Tau-pS214, Tau-pS324,
930 and Tau-pS214/pS324 (pS2) peptide binding to 14-3-3z (relates to Figure 1B). Data shown as
931 mean±SD, N=3 technical replicates per experiment.

932

933

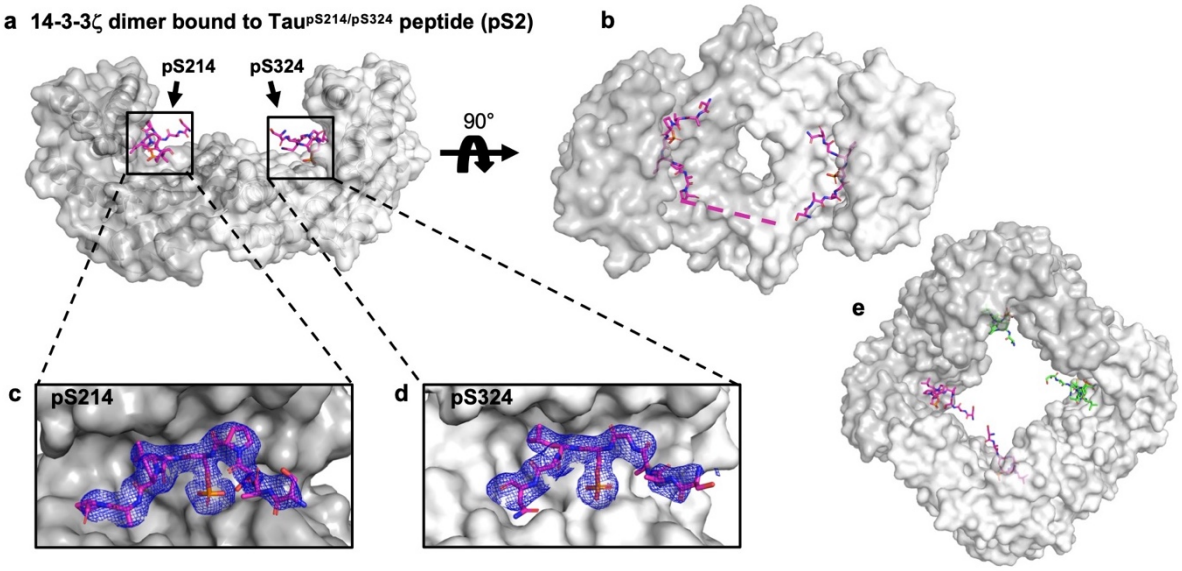

Extended Data Figure S2. Second 14-3-3ζ dimer part of the asymmetric unit in complex with Tau phospho-peptide pS2.

a, Cartoon plot with semi-transparent surface of the 14-3-3ζ dimer (gray) complexed with the pS214 and pS324 binding sites of the. pS2 Tau peptide (pink rods). **b,** Top view of pS214 and pS324 binding sites (pink rods) into the 14-3-3ζ binding grooves (grey semi-transparent surface). Pink dash line shows connective amino acid residues between the binding sites. **c+d,** Close-up of the binding grooves of monomer A and B (grey surface) containing the Tau peptide binding sites (pink rods). Final 2Fo-Fc electron density map of the peptide is shown (blue mesh, contoured at 1s). **e,** The crystal packing of the Tau pS2 peptide:14-3-3ζ crystal structure. Two 14-3-3ζ dimers are visible in gray semi-transparent surfaces. Two Tau pS2 peptides are shown as green and pink rods.

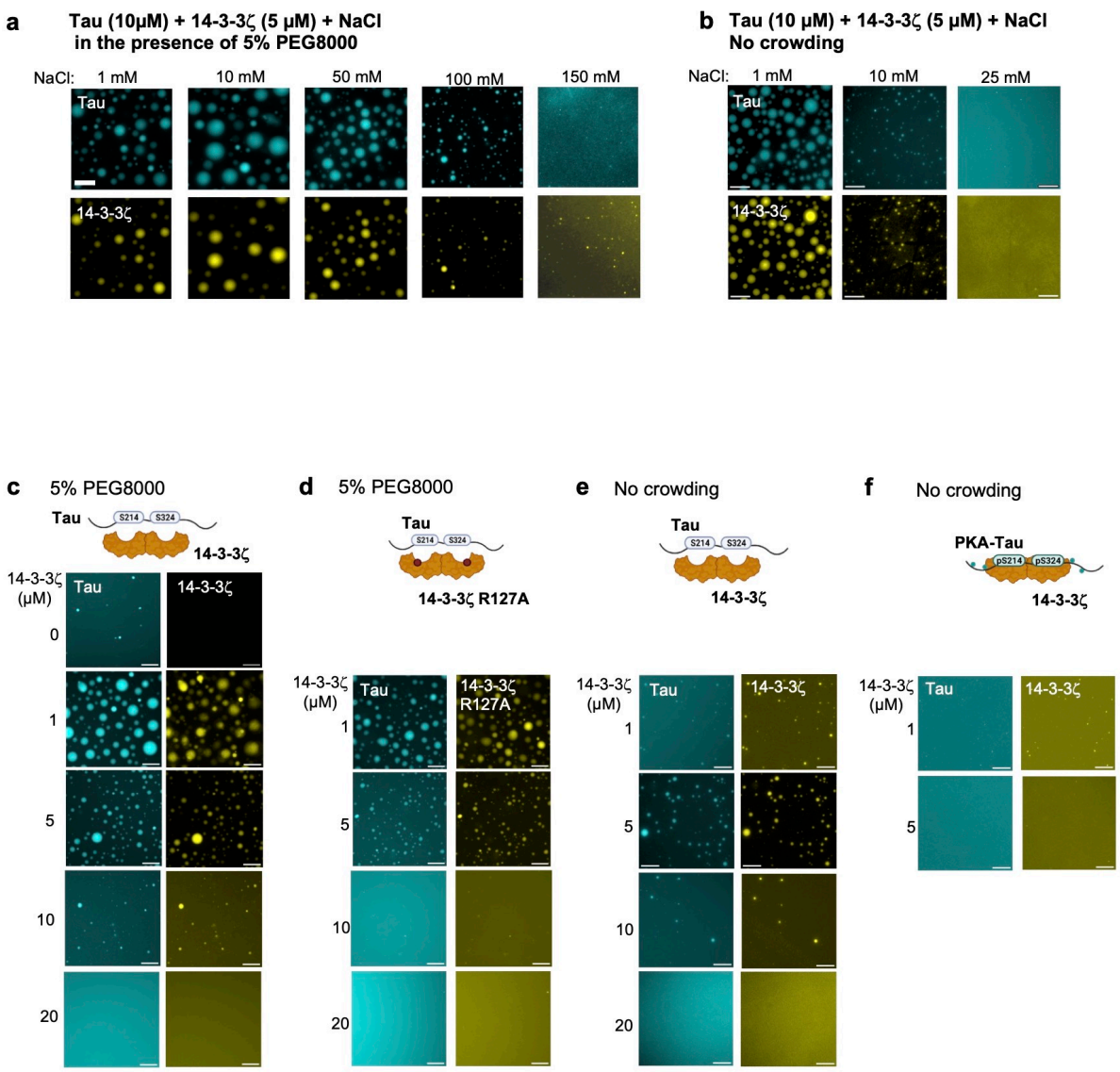

Extended Data Figure S3. Tau condensation triggered by 14-3-3ζ is inhibited by salt in the buffer.

a, Co-condensation of Tau with 14-3-3ζ in the presence of crowding agent PEG decreases with increasing NaCl concentrations in the assay buffer, suggesting that electrostatic interactions govern Tau:14-3-3z coacervation. Scale bars = 20 μM. **b,** 14-3-3ζ induced Tau condensation in the absence of crowding is reduced at NaCl concentrations of 10 □M, and inhibited at higher NaCl concentrations. Scale bars = 20 μM. **c+d,** Representative fluorescence microscopy images of 10 μM non-phosphorylated Tau with increasing 14-3-3ζ (A) and 14-3-3z R127A (B) concentrations (0, 1, 5, 10, 20 μM) in 25 mM HEPES, 1 mM DTT, pH 7.4 buffer in the presence of 5% (w/v) PEG. 2% Tau labeled with DyLight488, 2% 14-3-3ζ labeled with DyLight647. Scale bars = 20 μM. **e,** In the absence of the molecular crowding, 14-3-3ζ induces condensation of Tau (10 μM) in a concentration dependent manner, with the strongest condensation occurring at a 2:1 (Tau:14-3-3ζ) ratio. Scale bars = 20 μM. **f,** *In vitro* phosphorylation of Tau with PKA inhibits co-condensation of Tau (10 μM) and 14-3-3ζ at substoichiometric 14-3-3 concentrations in the absence of crowding. Scale bars = 20 μM.

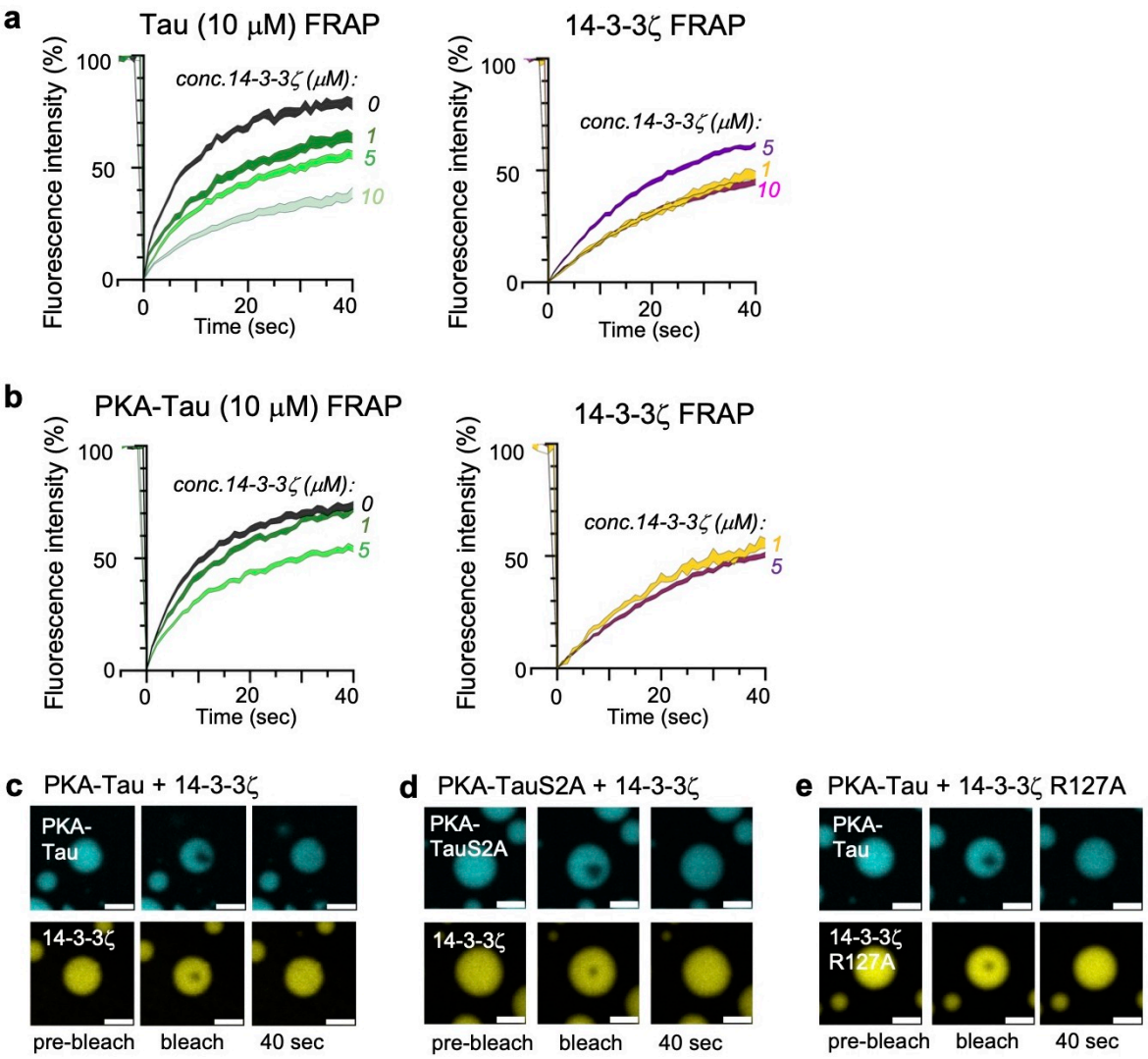

Extended Data Figure S4. FRAP images and curves of condensates formed from Tau and PKA-Tau and 14-3-3ζ variants and concentrations.

a, FRAP of Tau (10 μM; Tau with 2% Tau-Dylight488) and 14-3-3ζ (0-10 μM; with 2% 14-3-3ζ-DyLight650) condensates formed at different 14-3-3ζ concentrations**.** N=10-18 condensates per condition. Data shown as mean±SEM. **b,** FRAP of PKA-Tau (10 μM; Tau with 2% Tau-Dylight488) and 14-3-3ζ (0-10 μM; with 2% 14-3-3ζ-DyLight650) condensates formed at different 14-3-3ζ concentrations condensates formed at different 14-3-3ζ concentrations (0, 1, 5 μM). N=11-20 condensates per condition. Data shown as mean±SEM. **c,d,e,** Representative images of condensates formed from fluorescently labeled Tau-DyLight488 (10 μM, with 2% Tau-Dylight488) and 14-3-3ζ -DyLight650 (5 μM, with 2% 14-3-3ζ-DyLight650) variants right before and after photobleaching with the respective laser, and after 40 sec of recovery. Condensates formed in 25 mM HEPES, 1 mM DTT, pH 7.4 in the presence of 5% PEG. Scale bars =5 μm.

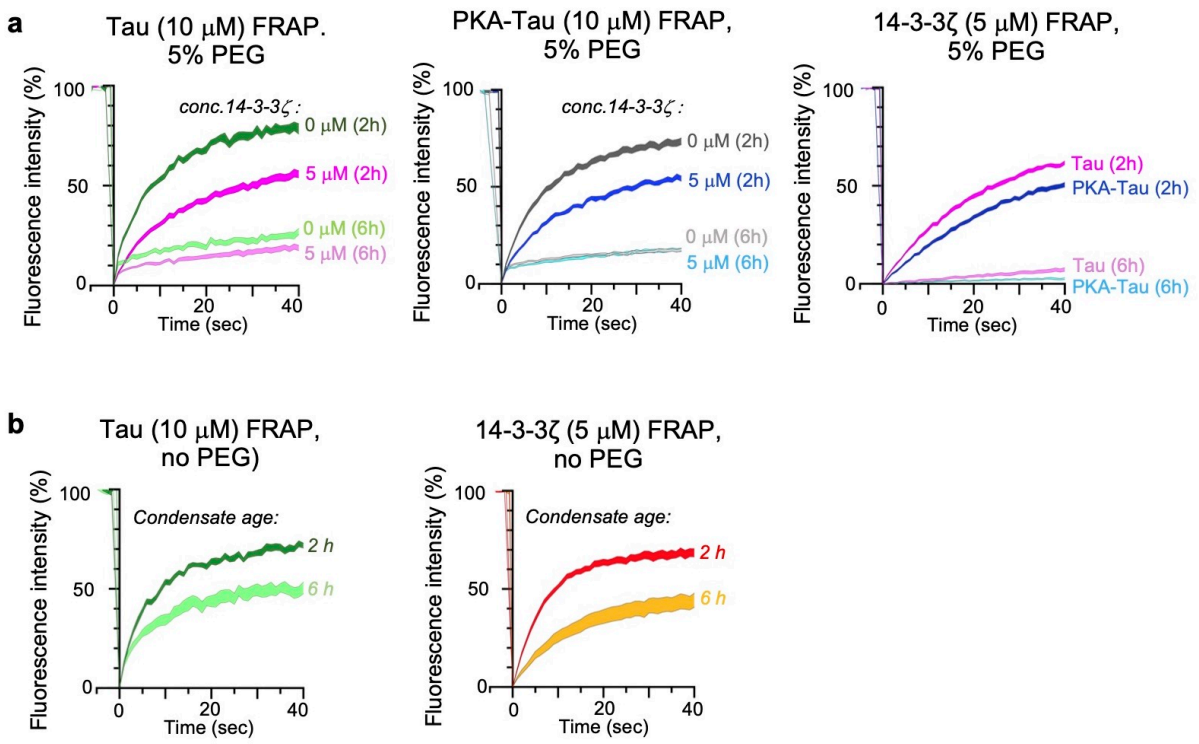

Extended Data Figure S5. 14-3-3ζ does not inhibit Tau condensate gelation (in the presence of crowding agent).

a, FRAP of "aging" Tau (10 μM; Tau with 2% Tau-Dylight488, left panel) or PKA-Tau (10 μM; Tau with 2% Tau-Dylight488, middle panel) condensates formed in 25 mM HEPES, 1 mM DTT, pH 7.4 in the presence of 5% PEG and with or without 14-3-3ζ (0 or 5 μM; with 2% 14-3-3ζ-DyLight650). FRAP of 14-3-3ζ is shown in the right panel. Condensates were analyzed at 2 h and 6 h after formation. N=15-18 condensates per condition. Data shown as mean±SEM.

b, FRAP of Tau (10 μM; with 2% Tau-Dylight488) and 14-3-3ζ (5 μM; with 2% 14-3-3ζ-DyLight650) condensates at 2 h and 6 h after formation in 25 mM HEPES, 1 mM DTT, pH 7.4 in the absence of PEG. N=11-15 condensates per condition. Data shown as mean±SEM.

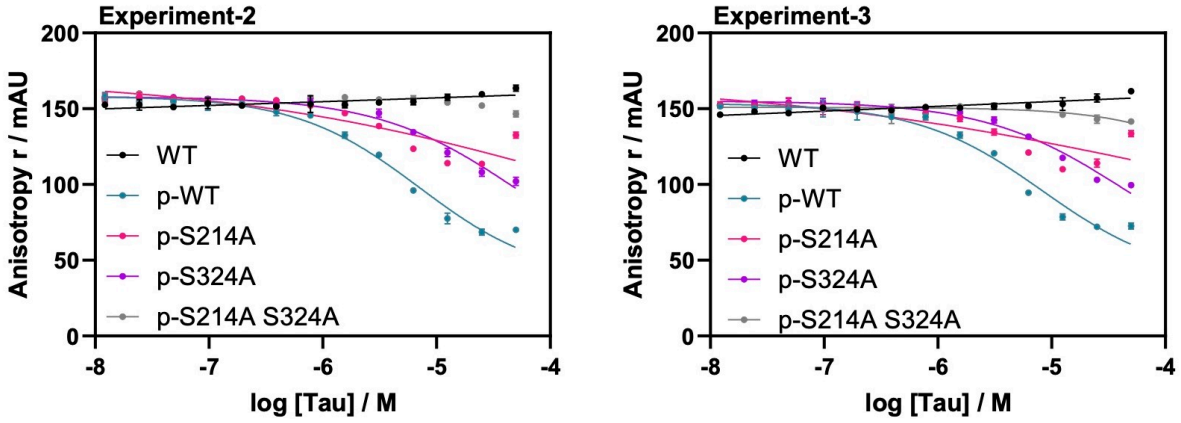

Extended Data Figure S6. Anisotropy of competition between phospho-Tau variants and pS2-FITC for the binding to 14-3-3ζ.

Independent experimental replicates of fluorescence anisotropy measurements for PKA-Tau variants competing with pS2-FITC bound to 14-3-3ζ (relates to Figure 4B). Data shown as mean±SD, N=3 technical replicates per experiment.

1007 **Extended Data Table 1. Data collection and refinement statistics of the crystal**
1008 **structure.** Statistics for the highest-resolution shell are shown in parentheses.
1009

PDB	**8QDV**
Protein	14-3-3ζΔc
Peptide/Ligand	$Tau^{pS214/pS324}$
Beam	ESRF ID23-1
Data collection	
Wavelength (Å)	0.972425
Space group	C 1 2 1
Cell dimensions a, b, c (Å) α, β, γ (°)	 152.45 ; 59.90 ; 146.67 90.00 ; 113.18 ; 90.00
Resolution (Å)	137.59-2.50
I / σ(I)	8.1 (1.3)
Completeness (%)	99.6 (99.9)
Redundancy	3.8 (3.6)
$CC_{1/2}$	0.996 (0.837)
Refinement	
No. reflections	43216
R_{work}/R_{free}	0.216/0.252
No. atoms Protein (Chain A, B, E, G) Peptide (Chain C, F) Water	 3542, 3474, 3360, 3473 213, 204 5
B-factors Protein (Chain A, B, E, G) Peptide (Chain C, F) Water	 71.9, 82.7, 89.4, 95.1 95.7, 107.7 66.4
R.m.s. deviations Bond lengths (Å) Bond angles (°)	 0.0053 1.127
Ramachandran favored (%) outliers (%)	 99 0.00

1010
1011
1012
1013